Journal of Power Sources 195 (2010) 4494–4512

Contents lists available at ScienceDirect

Journal of Power Sources

journal homepage: www.elsevier.com/locate/jpowsour

Influence of residual elements in lead on oxygen- and hydrogen-gassing rates of lead-acid batteries

L.T. Lam*, H. Ceylan, N.P. Haigh, T. Lwin, D.A.J. Rand

CSIRO Energy Technology, Bayview Avenue, Clayton South, Victoria 3169, Australia

ARTICLE INFO

Article history:
Received 12 November 2009
Received in revised form 7 December 2009
Accepted 7 December 2009
Available online 29 December 2009

Keywords:
Battery oxide
Gassing rate
Hydrogen
Oxygen
Residual element
Valve-regulated lead-acid battery

ABSTRACT

Raw lead materials contain many residual elements. With respect to setting 'safe' levels for these elements, each country has its own standard, but the majority of the present specifications for the lead used to prepare battery oxide apply to flooded batteries that employ antimonial grids. In these batteries, the antimony in the positive and negative grids dominates gassing characteristics so that the influence of residual elements is of little importance. This is, however, not the case for valve-regulated lead-acid (VRLA) batteries, which use antimony-free grids and less sulfuric acid solution. Thus, it is necessary to specify 'acceptable' levels of residual elements for the production of VRLA batteries. In this study, 17 elements are examined, namely: antimony, arsenic, bismuth, cadmium, chromium, cobalt, copper, germanium, iron, manganese, nickel, selenium, silver, tellurium, thallium, tin, and zinc. The following strategy has been formulated to determine the acceptable levels: (i) selection of a control oxide; (ii) determination of critical float, hydrogen and oxygen currents; (iii) establishment of a screening plan for the elements; (iv) development of a statistical method for analysis of the experimental results. The critical values of the float, hydrogen and oxygen currents are calculated from a field survey of battery failure data. The values serve as a base-line for comparison with the corresponding measured currents from cells using positive and negative plates produced either from the control oxide or from oxide doped with different levels of the 17 elements in combination. The latter levels are determined by means of a screening plan which is based on the Plackett–Burman experimental design. Following this systematic and thorough exercise, two specifications are proposed for the purity of the lead to be used in oxide production for VRLA technology.

1. Background

Valve-regulated lead-acid (VRLA) batteries, which require no water maintenance, have increasingly replaced conventional flooded batteries in stationary applications, e.g., in telecommunications and uninterruptible power-supply systems. Nevertheless, it has been found [1–4] that the endurance of VRLA batteries under such applications can be much shorter than the design life, which is typically 20 years. The main failure modes of these batteries are as follows: dry-out and thermal runaway, selective discharge of negative or positive plates, heavy grid corrosion, and positive-plate failure (Fig. 1). While there are several possible causes for a given failure mode, it is clear that residual elements can exert a strong influence on all failure modes through gassing effects. Thus, obviously, controlling of the influence of residual elements on gassing rates to within the safe limits is a key strategy for improving the life of VRLA batteries. Moreover, sure knowledge of these limits will avoid the unnecessary ultra-refining of lead.

Raw lead materials contain many residual elements. Some elements may promote high gassing, and/or grid corrosion, and/or shedding of positive material. Others may improve the connectivity of the positive active material, and/or enhance the corrosion resistance, and/or exert little influence on gassing characteristics. This investigation first examined the influence of: antimony (Sb), arsenic (As), bismuth (Bi), cadmium (Cd), chromium (Cr), cobalt (Co), copper (Cu), germanium (Ge), iron (Fe), manganese (Mn), nickel (Ni), selenium (Se), silver (Ag), tellurium (Te), tin (Sn), and zinc (Zn). Later, thallium (Tl) was added to this list of elements.

To improve battery performance, it is necessary to identify those elements which give rise to appreciable hydrogen and/or oxygen gassing and which, therefore, must be restricted or avoided as 'harmful elements'. Ag, As, Co, Cr, Cu, Fe, Mn, Ni, Sb, Se and Te are regarded as harmful elements because they are known to promote hydrogen and/or oxygen gassing. On the other hand, Bi, Cd, Ge, Sn, and Zn, which are known/expected to enhance battery performance, are considered to be 'beneficial elements'. (Note that there

* Corresponding author at: CSIRO Energy Technology, Gate 1, Normanby Road, Box 312, Clayton South, Victoria 3169, Australia. Tel.: +61 3 95458986; fax: +61 3 95628919.
E-mail address: Lan.Lam@csiro.au (L.T. Lam).

0378-7753/$ – see front matter © 2009 Elsevier B.V. All rights reserved.
doi:10.1016/j.jpowsour.2009.12.020

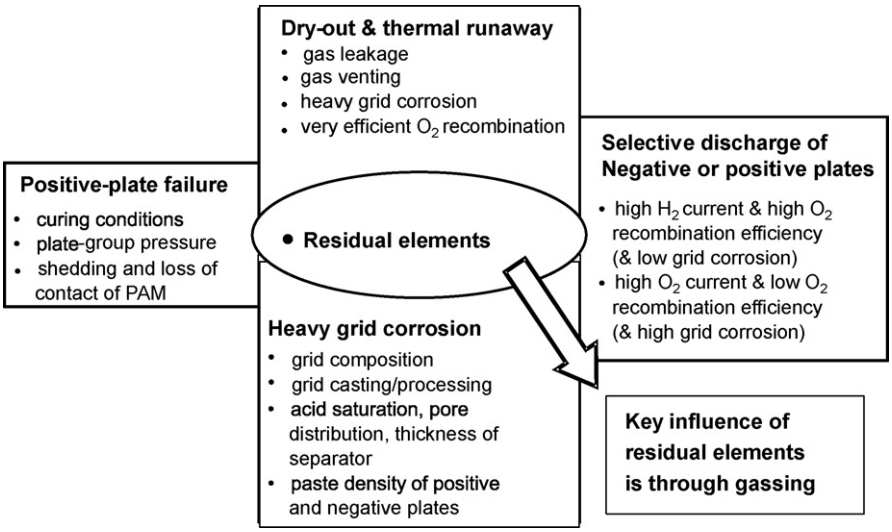

Fig. 1. Failure modes of VRLA batteries under stationary applications.

appears to be little information on the influence of Tl on gassing rates.) It is understood that some of the elements examined in this study may not be present in the lead produced by some companies. Nevertheless, since these elements are likely to occur in secondary (recycled) lead – the other major lead resource for battery production – a plan for determining the maximum acceptable levels (MALs) for all of the selected residual elements has been developed. In this study, the residual elements were added to the control oxide in a powdered oxide form. It may be argued that it is unnecessary to examine the effects of Mn and Ge because these elements usually do not exist in refined lead. Nevertheless, these two elements are also included in an attempt to explore, if any, their prospective beneficial properties.

With respect to setting 'safe' levels for residual elements in lead, each country has adopted its own standard specification. The majority of these standards have, however, focused on battery technologies that employ antimonial grid alloys (Table 1). In these designs, the antimony in the positive and negative grids dominates the performance of the battery so that the influence of residual elements (either harmful or beneficial) is of little importance. Consequently, some harmful elements such as Co, Cr, Mn and Ni have not been included in the various national standards for lead. By contrast, VRLA batteries employ non-antimonial alloys, such as lead–calcium–tin and lead–tin with or without the incorporation of silver, to increase the corrosion resistance of positive grids. Thus, as the market for VRLA technology increases, less antimony will be required for the manufacture of lead-acid batteries and more silver and tin will be used. Consequently, the levels ('arisings') of these latter two elements in recycled lead will increase and will become greater than those specified in existing standards. This raises major issues for lead producers. For example, silver can reduce the rate of production of leady oxide via the Barton-pot process by up to 10% [5]. It is also very costly to remove low levels of silver from secondary lead. Clearly, it is essential to determine the maximum acceptable levels of all residual elements – especially silver and tin – in lead used for the manufacture of VRLA batteries.

Given the above considerations, the objective of this study is to enhance the performance of VRLA batteries on stand-by (float) duty by controlling any influence of residual elements in lead raw materials on hydrogen- and/or oxygen-gassing rates to safe limits through:

(i) determination of the maximum acceptable levels (MALs) of residual elements;
(ii) optimization of the influence of prospective beneficial elements such as bismuth, cadmium, germanium, tin, and zinc;
(iii) development of specifications for acceptable levels of residual elements.

2. Overall strategy

In order to achieve the above objective, an overall strategy has been formulated to undertake the following four key actions.

(i) It is necessary to identify and to determine the safe limits. These limits are the critical values of the float, hydrogen and oxygen currents that can be sustained by VRLA batteries with a design life of, typically, 20 years in float service. Each current should be determined and then used as a base-line.
(ii) Since there are 17 elements to be examined, a screening plan, which can provide maximum outcome with minimum effort, must be developed.
(iii) An experimental procedure should be devised to measure the float, hydrogen and oxygen currents from cells prepared from control oxide and oxides doped with residual elements in combination.
(iv) A data-analysis procedure should be established to determine the levels of individual elements at which the measured float, hydrogen and oxygen currents are equal to the corresponding critical values. Specifically, for each element, there are three relevant concentrations, namely, one for float current, one for hydrogen current, and one for oxygen current. Nevertheless, the lowest concentration will be taken as the MAL for that element.

Lead produced by the Doe Run Company is chosen for preparation of the control oxide to which the residual elements are added. This is because Doe Run lead is of high purity.

3. Critical float, hydrogen- and oxygen-evolution currents

Brecht [6] has found that conventional, non-antimonial, flooded batteries used in stand-by applications can typically experience between 40 and 65% corrosion of the positive grid by the end of life. In addition, Brecht has calculated that for a VRLA battery, conversion of 50% of the grid metal to PbO_2 will produce a corresponding 20% reduction in the level of acid saturation of the separator, i.e., from 95 to 75%. This usually results in a 40%, or greater, loss of

Table 1
Standard and proposed specifications (ppm) for lead used in the production of VRLA batteries.

Elements	Present specified levels					Pasminco VRLA Refined™ lead
	AS 1812 (1975) Pb 99.99	ASTM B29 (1992) Refined pure	BS 334 (1982) Type A	DIN 1719 (1986) Pb 99.99	USA	
Beneficial element						
Bi	5	25	5	5	500	500
Harmful elements						
As	10	5	5	10	20	1
Ba	ns[a]	ns	ns	ns	ns	10
Co	[b]	ns	ns	ns	ns	1
Cr	ns	ns	ns	ns	ns	5
Fe	10	10	30	10	20	5
Mn	ns	ns	ns	ns	ns	3
Mo	ns	ns	ns	ns	ns	3
Ni	[b]	2	10	ns	ns	2
Sb	10	5	20	10	20	1
Se	ns	ns	ns	ns	ns	1
Te	ns	ns	ns	ns	ns	0.3
V	ns	ns	ns	ns	ns	4
Other elements						
Ag	10	25	25	10	15	10
Cd	10	ns	ns	ns	ns	5
Cu	10	10	30	10	15	10
Ge	ns	ns	ns	ns	ns	5
Sn	10	ns	5	ns	ns	10
Zn	10	ns	20	10	10	5

[a] ns = not specified.
[b] Co + Ni < 10 ppm.

useable capacity. Thus, with the same degree of grid corrosion, the VRLA battery will fail because of electrolyte dry-out, and not because of grid corrosion. Now, let us assume that VRLA batteries reach the end of life (i.e., 20 years) when at least half of the original grid metal is converted to PbO_2 through the following reaction

$$Pb + 2H_2O \rightarrow PbO_2 + 4H^+ + 4e^- \quad (1)$$

Accordingly, the amount of water required to corrode 50% of the positive-grid material in a VRLA battery with, for example, a $C_3/3$ capacity of 100 Ah (total positive-grid weight = 1572 g per cell; amount of H_2SO_4 (1.285 rel.dens.) = 1414.7 g per cell; amount of H_2O = 877.1 g per cell) is calculated to be 0.068 g Ah^{-1} per cell per year. This is equivalent to a hydrogen-evolution current of 0.023 mA Ah^{-1} per cell. During float charging of batteries, the corrosion current is generally 2–2.6% of the float current [1,7]. Using the average value of 2.3%, the float and oxygen-evolution currents delivered by the above VRLA battery will be 1.0 and 0.977 mA Ah^{-1} per cell, respectively. This value of the float current is the same as that reported by Harrison [8]. Surprisingly, there is also good agreement with the observations of Jones et al. [9] on VRLA batteries fitted with catalysts (float current = 1.0–1.4 mA Ah^{-1} per cell). These latter batteries are claimed to last for 20 years.

In summary, the above analysis shows that to achieve a life of 20 years from a conventional VRLA with ~100% recombination efficiency, the critical hydrogen-/oxygen-evolution currents and float current are as follows:

$$I_{\text{float critical}} = 1.000\ \text{mA Ah}^{-1}\ \text{per cell} \quad (2)$$

$$I_{\text{H}_2\text{critical}} = 0.023\ \text{mA Ah}^{-1}\ \text{per cell} \quad (3)$$

$$I_{\text{O}_2\text{critical}} = 0.977\ \text{mA Ah}^{-1}\ \text{per cell} \quad (4)$$

These critical currents are used as the base-line for the determination of the MALs of both harmful and beneficial elements when added to the control oxide. Since the oxygen-recombination efficiency is close to 100%, it should be noted that the critical hydrogen-evolution current is equal to the current due to grid corrosion. The values of this current given in this study are expressed as mA per Ah at the 3-h rate and, therefore, will be greater than values reported by other authors [1,10] who have cited mA per Ah at 5- to 10-h rates.

4. Screening plan—Plackett–Burman experimental design

The effect of residual elements on the rate of hydrogen evolution at the negative plate in a lead-acid system is considered to decrease in the order:

Ni > Sb > Co > Cr > Fe > Mn > Cu > Se > Te > As
> Sn > Ag > Bi > Ge > Zn > Cd

Clearly, for each element, there is a MAL of its concentration beyond which the element will cause unacceptable rates of hydrogen and/or oxygen. The aim, now, is to determine the MALs for the initially selected, 16 residual elements (as mentioned in Section 1, Tl was added into this matrix in the later stage of the work program). Obviously, the Lower Levels are the actual levels of residual elements that are present in the Doe Run oxide. None of the MALs are accurately known and, therefore, it is necessary to start the experimentation using the best approximation based on existing knowledge. The following iterative procedure is adopted to identify the desired MALs of the residual elements.

For harmful elements, the first approximations to the MALs are taken from the experiments Prengaman on flooded batteries [11]. For beneficial elements, the first approximations of the MALs are deliberately increased to 500 ppm. The initial Upper Level – Upper Level (1), the first approximation of the MALs – of each of the 16 elements is given in Table 2.

The Plackett–Burman design has been chosen to determine the MALs of the 16 residual elements because it has been widely and successfully used by many industries to screen large numbers of variables with a minimal effort. The reason why this design is used is explained, by way of example, in Fig. 2. For simplicity, only three elements (i.e., Ni, Sb and Co) are considered and are each screened at two levels, namely low (L) and high (H). With a con-

Table 2
First Plackett–Burman design: initial approximation of MALs–Upper Level (1).

Residual elements	Lower Level[a] (ppm)	Upper Level (1) (ppm)
Ni	<1.0	10.0
Sb	<1.0	10.0
Co	<1.0	10.0
Cr	<1.0	5.0
Fe	1.3	10.0
Mn	<1.0	3.0
Cu	<1.0	10.0
Ag	4.0	20.0
Se	<0.5	1.0
Te	<0.3	0.3
As	<1.0	10.0
Sn	<1.0	10.0
Bi	<1.0	500.0
Ge	<1.0	500.0
Zn	<1.0	500.0
Cd	<1.0	500.0

[a] The Lower Levels are the concentrations of residual elements in Doe Run 'control' oxide. Note that, the lower level for Tl is 10 ppm (the upper level for this element was addressed later in the project).

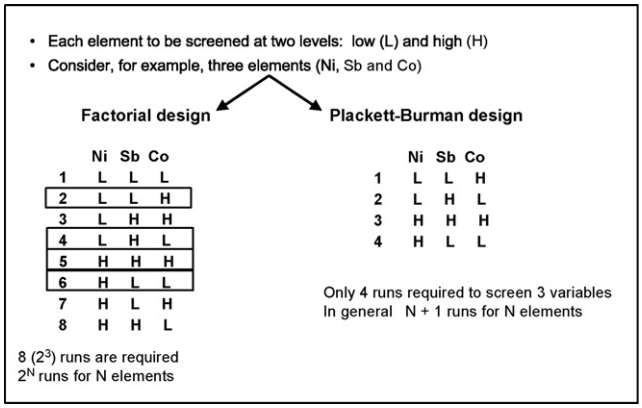

Fig. 2. Advantages of Plackett–Burman design.

ventional factorial design, the levels of the three elements can be set in eight different ways, i.e., all elements at low levels, nickel and antimony at low level but cobalt at high level, and so on. In general, 2^N runs will be required to screen N variables. Thus, evaluation of 16 elements will require 65,536 runs—an impossible task! By contrast, the Plackett–Burman design can be used to determine separately either the maximum levels or the minimum levels of residual elements. Furthermore, the advantage of this design is that the determination of either maximum or minimum levels of three elements requires only four runs (Fig. 2). In general, $N+1$ runs are required to evaluate the effects of N elements. This procedure is applicable for cases where $N+1$ is a multiple of 4 [12]. Thus, there are options to screen 7 elements with 8 experiments (7/8 plan), 11 elements with 12 experiments (11/12 plan), 15 elements with 16 experiments (15/16 plan), and so on. Accordingly, 17 experiments would be required to screen the effects of 16 elements on the hydrogen- and oxygen-gassing rates. Obviously, this number of experiments is not a multiple of 4. Therefore, a 19/20 plan should be used. In fact, 27 runs were conducted and these included repeat trials as well as some drift-check trials to determine the tolerance of the experimentation. Using the values for Upper Level (1) from Table 2, the complete Plackett–Burman design for 16 elements at two concentrations is presented in Table 3. The combined levels of the 16 elements define an experimental run. Trial #1 is to check the control oxide. Trials #2 and #3 determine the gassing behaviour of oxide when doped with all 16 residual elements at high- and mid-levels. Trials #13 and #25 are repeats of trial #1. Trials #14 and #26 are repeats of trial #2. Finally, trial #27 is a repetition of trial #6.

The Plackett–Burman design can only provide the main effect (i.e., single variable effect) of each of the 16 elements considered. It cannot provide 'synergistic' effects caused by two or more

Table 3
First Plackett–Burman design of 16 elements (concentration, ppm) with repeat trials.

Trial No.	Ni	Sb	Co	Cr	Fe	Mn	Cu	Ag	Se	Te	As	Sn	Bi	Ge	Zn	Cd	Run order
1	0	0	0	0	0	0	0	0	0	0	0	0	0	0	0	0	1
2	10	10	10	5	10	3	10	20	1	0.3	10	10	500	500	500	500	2
3[a]	5	5	5	2.5	3	1.5	5	10	0.5	0.15	5	5	250	250	250	250	3
4	10	10	0	0	10	3	10	20	0	0.3	0	10	0	0	0	0	9
5	10	0	0	5	10	3	10	0	1	0	10	0	0	0	0	500	24
6	0	0	10	5	10	3	0	20	0	0.3	0	0	0	0	500	500	12
7	0	10	10	5	10	0	10	0	1	0	0	0	0	500	500	0	11
8	10	10	10	5	0	3	0	20	0	0	0	0	500	500	0	500	16
9	10	10	10	0	10	0	10	0	0	0	0	10	500	0	500	500	7
10	10	10	0	5	0	3	0	0	0	0	10	10	0	500	500	0	21
11	10	0	10	0	10	0	0	0	0	0.3	10	0	500	500	0	0	5
12	0	10	0	5	0	0	0	0	1	0.3	0	10	500	0	0	500	19
13[b]	0	0	0	0	0	0	0	0	0	0	0	0	0	0	0	0	13
14[c]	10	10	10	5	10	3	10	20	1	0.3	10	10	500	500	500	500	14
15	10	0	10	0	0	0	0	20	1	0	10	10	0	0	500	500	20
16	0	10	0	0	0	0	10	20	0	0.3	10	0	0	500	500	500	18
17	10	0	0	0	0	3	10	0	1	0.3	0	0	500	500	500	500	10
18	0	0	0	0	10	3	0	20	1	0	0	10	500	500	500	0	22
19	0	0	0	5	10	0	10	20	0	0	10	10	500	500	0	500	6
20	0	0	10	5	0	3	10	0	0	0.3	10	10	500	0	500	0	8
21	0	10	10	0	10	3	0	0	1	0.3	10	10	0	500	0	500	4
22	10	10	0	5	10	0	0	20	1	0.3	10	0	500	0	500	0	17
23	10	0	10	5	0	0	10	20	1	0.3	0	10	0	500	0	0	15
24	0	10	10	0	0	3	10	20	1	0	10	0	500	0	0	0	23
25[b]	0	0	0	0	0	0	0	0	0	0	0	0	0	0	0	0	26
26[c]	10	10	10	5	10	3	10	20	1	0.3	10	10	500	500	500	500	25
27[d]	0	0	10	5	10	3	0	20	0	0.3	0	0	0	0	500	500	27

[a] All elements at mid-levels.
[b] Repeat of trial #1.
[c] Repeat of trial #2.
[d] Repeat of trial #6.

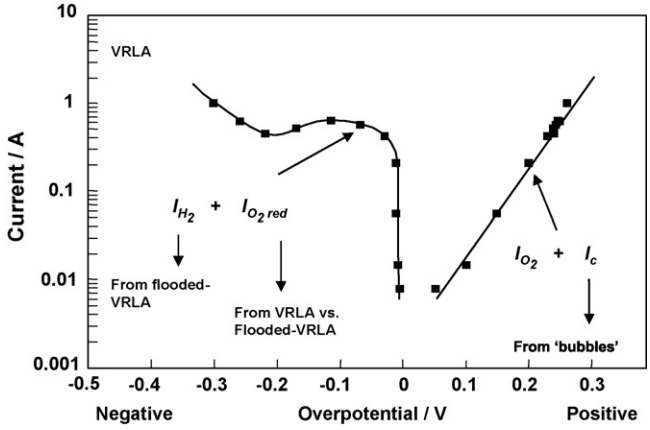

Fig. 3. Electrochemical characteristics of VRLA batteries.

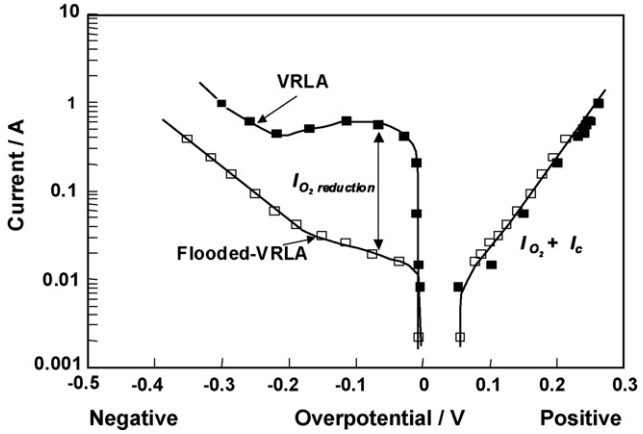

Fig. 5. Determination of oxygen-reduction current.

elements. (Note, 'synergy' is commonly used to describe an advantageous outcome, but in the present case the result could be disadvantageous. Therefore, the terms 'beneficial synergy' and 'detrimental synergy' are used to distinguish between these two opposite situations.) From inspection of individual trials, possible beneficial or detrimental synergistic effects between elements can be qualitatively estimated and explored, in addition to resolution of the main effects.

5. Determination of electrochemical characteristics

It is well known that oxygen evolution and grid corrosion occur simultaneously at the positive plates during the overcharge of both flooded and VRLA cells. Hydrogen evolution is the predominant reaction at the negative plates in flooded cells, but is accompanied by oxygen reduction in VRLA designs (Fig. 3, data obtained from Ref. [13]). Therefore, in order to determine the separate rates of these two reactions at the negative plate in a given VRLA cell, the oxygen-reduction process has to be suppressed in a parallel experiment performed with the same cell. This can be achieved by minimizing the transport of oxygen from the positive plate through: (i) assembling the cell with no compression; (ii) inserting polyethylene separators with ribs facing the positive plates; (iii) flooding the cell with acid. To distinguish a cell prepared under such conditions from a conventional flooded type, the cell is referred to as a 'flooded-VRLA' design. The current–overpotential behaviour of such a cell is shown in Fig. 4. The current at the negative plate is now consumed only by hydrogen evolution. The difference in the negative-plate current between the VRLA and the flooded-VRLA cell at the same overpotential is the oxygen-reduction current (Fig. 5). For positive plates, the current in both cell designs (VRLA or flooded-VRLA) is the combined current of oxygen evolution and grid corrosion (Fig. 5). Thus, to obtain the oxygen-evolution current, the corrosion current has to be determined separately (i.e., by 'bubble' experiments, see Section 5.2).

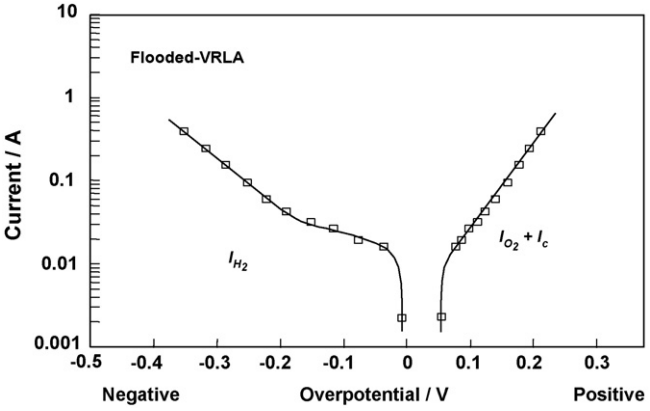

Fig. 4. Current–potential behaviour of a flooded-VRLA battery.

Table 4
Paste formulae for test electrodes.

Component	Negative electrode	Positive electrode
Leady oxide (kg)	1	1
Fibre (g)	0.6	0.3
$BaSO_4$ (g)	4.93	–
Carbon back (g)	0.26	–
H_2SO_4, 1.400 rel.dens. (cm^3)	57	57
Water (cm^3)	110	130
Acid-to-oxide ratio (%)	4	4
Paste density ($g\,cm^{-3}$)	4.7	4.5

5.1. Construction of electrodes

Negative- and positive-pasted plates were made from Doe Run oxide, as well as from this oxide doped with a combination of elements at the levels given in Table 3. Note that the concentrations of elements in the Doe Run oxide that are less than 1 ppm (see Table 2) were ignored when adding these elements to the required levels listed in Table 3. This is permissible because the 'true' acceptable levels of the residual elements will be slightly higher than those specified by the present study.

The paste formulae for the negative and the positive electrodes are presented in Table 4. For pastes prepared from control oxide doped with different levels of residual elements, the mixture of dried powders was placed in a plastic container. The container was then shaken for about 30 min before undertaking paste preparation. To exclude any contamination from the sulfuric acid required for paste mixing and battery electrolyte, analytical grade reagent was used throughout the entire experimental programme.

The paste was applied to positive and negative grids that had the dimensions and alloy compositions listed in Table 5. The pasted

Table 5
Dimensions and composition of negative and positive grids.

	Negative grid	Positive grid
Height (mm)	68	68
Width (mm)	40	40
Thickness (mm)	3.3	3.3
Composition	Pb–0.09 wt.% Ca–0.3 wt.% Sn	Pb–0.09 wt.% Ca–0.8 wt.% Sn

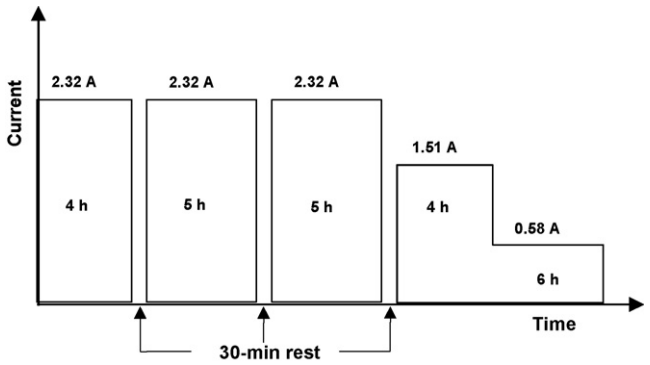

Fig. 6. Formation profile for battery plates.

plates were cured at 50 °C and 100% relative humidity for 24 h, and then dried at 60 °C and ambient humidity for 8 h. After processing, two positive and two negative plates, together with separator sheets, were assembled into 2-V cells. Dilute sulfuric acid (1.07 rel.dens.) was introduced and the cell was allowed to stand for at least 30 min. The formation was conducted using the profile shown in Fig. 6. Three rest periods of 30 min were included to facilitate the diffusion of acid into the interior of the plates. After formation, the electrolyte was adjusted to ~1.285 rel.dens. by the addition of concentrated sulfuric acid (1.83 rel.dens.). The cell was 'conditioned' by applying 5–15 repetitive cycles with discharge at the 3-h rate. After full charging, the plates were used to determine the grid corrosion, hydrogen-evolution and oxygen-evolution currents.

5.2. Determination of grid corrosion

In general, grid corrosion is evaluated by means of a weight-loss procedure, i.e., the amount of corrosion is taken to be the difference in the weight of the grid before the corrosion test and after the corrosion layer has been removed via dissolution. The accuracy of this procedure is dependent on the structural homogeneity of the grid alloy. A homogeneous structure, such as a high-antimony lead alloy, will favour uniform corrosive attack throughout the entire metal surface (i.e., general corrosion). In this case, complete digestion of corrosion layer is to be expected. By contrast, a heterogeneous structure, such as found with low-antimony or lead–calcium–tin alloys, will suffer preferential attack at the grain boundaries of the metal surface and thereby give rise to penetration corrosion. Under such conditions, there will be incomplete dissolution of the corrosion layer and this will lower the accuracy of results obtained via the weight-loss procedure. Therefore, given that the present study employs grids made from lead–calcium–tin alloys, an alternative 'bubble' method was employed to determine the rate of grid corrosion (Fig. 7).

An electrochemical cell was assembly with one fully charged positive and two fully charged negative plates in acid of 1.285 rel.dens. The potential of the positive plate was measured with a 5 M $Hg|Hg_2SO_4$ reference electrode. An inverted funnel was placed above the positive plate and was connected to a burette which was mounted horizontally. Prior to measurement, bubbles of detergent were introduced into the burette and a constant current was applied to the cell. The oxygen evolved from the positive plate was collected continuously by the inverted funnel and the increasing partial pressure promoted the movement of the bubbles in the burette. The rate of oxygen evolution is represented by the movement of detergent bubbles per unit time (i.e., volume change per unit time). The oxygen-evolution current was calculated using the following relationship

$$I_{O_2} = \frac{[4FV(P_{total} - P_w)]}{10^6 RTt} \quad (5)$$

where $F = 96\,500$ C mol^{-1}; V = gas volume (ml) collected in burette; $P_{total} = 101{,}325$ Pa; P_w = vapour pressure (Pa) at temperature T; R = gas constant = 8.31 J mol^{-1} K^{-1}; T = absolute temperature (K); t = duration of experiment (s).

Since the current at the positive plate is the combined value of oxygen evolution and grid corrosion, the latter current can be determined by

$$I_c = I_{applied} - I_{O_2} \quad (6)$$

The above experiment was conducted at various applied currents at 25, 45 and 65 °C.

The corrosion current of a positive plate using a Pb–0.09 wt.% Ca–0.8 wt.% Sn grid at different potentials and temperatures is shown in Fig. 8. There is a linear relationship between the corrosion current (logarithmic scale) and the positive-plate overpotential. This behaviour holds for all temperatures studied. The Tafel slopes increase with increase in temperature, namely, 63, 74 and 91 mV at 25, 45 and 65 °C, respectively. This behaviour indicates a change in the mechanism of grid corrosion.

5.3. Determination of hydrogen- and oxygen-evolution currents

The cell used to determine the hydrogen- and oxygen-evolution currents is shown in Fig. 9. The main apparatus was constructed

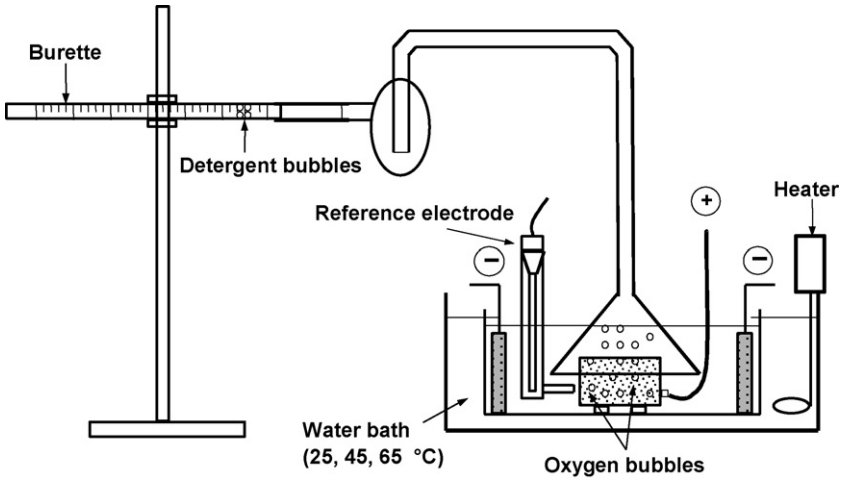

Fig. 7. Apparatus used to determine grid-corrosion and oxygen-evolution currents.

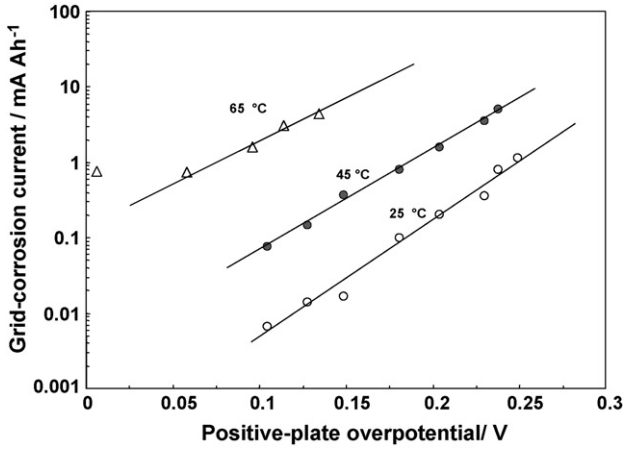

Fig. 8. Corrosion current of pasted Pb–0.09 wt.% Ca–0.8 wt.% Sn grid at different overpotentials and temperatures.

from polypropylene. The cell consists of a pasted-positive plate, a separator [absorptive glass-microfibre (AGM) or a combination of AGM and Daramic polyethylene], and a pasted-negative plate. A piston is arranged to move freely and is used to compress the plate group by turning a screw clockwise. The value of the plate-group pressure is measured by a load cell and can be adjusted by the screw. A plate-group pressure of 40 kPa was adopted.

5.3.1. Flooded-VRLA cells

Positive and negative plates of the type discussed in Section 5.1, together with a polyethylene separator, were assembled with no compression into a 2-V cell, as shown in Fig. 9. The cells were then fitted with a 5 M $Hg|Hg_2SO_4$ reference electrode and allowed to stand for at least 24 h for determination of the open-circuit voltage along with the negative-plate and positive-plate potentials. A voltage-step procedure was employed to determine the electrochemical characteristics of the cell. The method involved stepping the voltage of the cell to consecutive set values (i.e., 2.15, 2.20, 2.27, 2.30, . . ., 2.45 V); the cell was held at each voltage for either 10 h (for voltages less than 2.30 V) or 5 h (for voltages greater than 2.27 V). During this time, the positive- and negative-plate potentials, the internal pressure, and the delivered current were recorded continuously. The values obtained after 10 or 5 h were used to plot either the current–voltage curve for the cell or the current–overpotential curve (Tafel plot) for each plate polarity.

5.3.2. VRLA cells

Following the above voltage-step experiments, the polyethylene separator was removed and replaced with an AGM counterpart. The cell-group pressure was set at 40 kPa. Excess acid (i.e., that not retained by plates and separators) was decanted from the cells. At this stage, the level of acid saturation in the separator was considered to be 100%. To achieve the desired saturation of 95%, the plate-group pressure was further increased to 42 kPa so that the excess acid was squeezed from the separator. The plate-group pressure was then released back to 40 kPa. Current–voltage and current–overpotential curves were obtained by means of the same voltage-step procedure as that described above for flooded-VRLA cells.

6. Results and discussion

6.1. First Plackett–Burman design

6.1.1. Float, hydrogen and oxygen currents of control oxide

Current–voltage plots at 21 °C (room temperature) for flooded-VRLA and VRLA cells prepared from the control oxide are shown in Fig. 10. For the flooded-VRLA design, the cell exhibits a linear relationship between the current (logarithmic scale) and the cell voltage when the latter is in the range 2.27–2.45 V. By contrast, the VRLA assembly displays non-linear behaviour over the same voltage range, namely, the current increases initially with increase in voltage but starts to level off at 2.41 V. At all cell voltages, the current delivered by the VRLA cell is significantly higher than that delivered by its flooded equivalent.

In order to understand the cause(s) of the above difference in current–voltage behaviour, Tafel plots were obtained for the two plate polarities, see Fig. 11. The positive plates in both cell designs have similar Tafel characteristics with a slope of ~100 mV, i.e., a value which lies between those for oxygen evolution on α-PbO_2

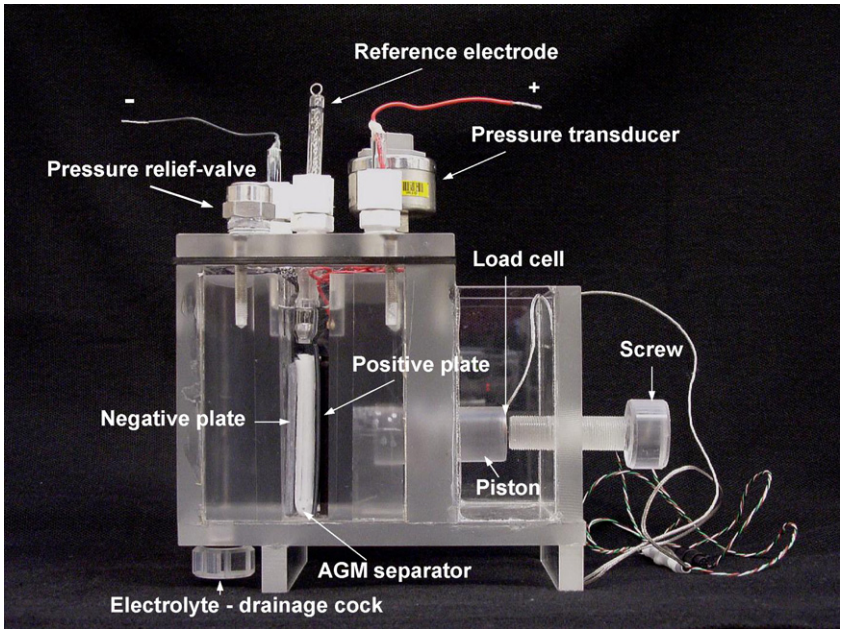

Fig. 9. Electrochemical cell used to determine hydrogen- and oxygen-evolution currents.

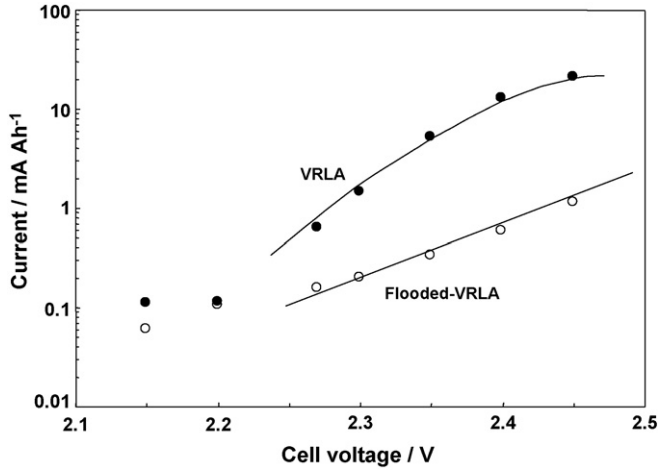

Fig. 10. Relationship between current and voltage for (○) flooded-VRLA and (●) VRLA cells at 21 °C.

and β-PbO_2 electrodes, viz., 70 and 140 mV, respectively [14]. The characteristics of negative plates in the flooded-VRLA cell differ markedly from those in the VRLA counterpart. The flooded-VRLA cell gives a Tafel plot with a slope of ~128 mV. Note, this value is slightly higher than the theoretical value for hydrogen evolution (i.e., 120 mV), a discrepancy which has been observed by other authors [15]. The relationship between the total current and the negative-plate overpotential in the VRLA cell is not linear and is due to the influence of the competing reaction of oxygen reduction. This accounts for the difference in current–voltage behaviour of the two types of cell. The overpotential of negative plates in the VRLA cell is small (i.e., 0.004–0.010 V) compared with that in the flooded-VRLA counterpart when both cells are charged at a low cell voltage (i.e., 2.21–2.36 V); a feature which has been reported by other workers [16,17]. At the same overpotential, the total current consumed by the negative plates is significantly higher in the VRLA cell. Obviously, the additional current in the VRLA battery is due to the reduction of oxygen. The float current delivered by the VRLA cell under constant-voltage charging at 2.27 V is 0.63 mA Ah^{-1}.

The float current at the positive plate is equal to the combined currents of oxygen evolution and grid corrosion, i.e.,

$$I_{float} = I_{O_2} + I_c \quad (7)$$

The value of I_c at the overpotential of the positive plate (i.e., 0.14 V, Fig. 11) of the VRLA cell when float charging at 2.27 V can be determined from Fig. 9 and is found to be 0.022 mA Ah^{-1}. Accordingly, from Eq. (7), the oxygen-evolution current is 0.63–0.022 = 0.608 mA Ah^{-1}.

The float current at the negative plate of the VRLA cell when charging at 2.27 V is the combination of the hydrogen-evolution and oxygen-reduction currents, namely:

$$I_{float} = I_{H_2} + I_{O_2\,reduction} \quad (8)$$

To obtain the hydrogen-evolution current, a straight line is drawn perpendicularly at the negative-plate overpotential of the VRLA cell to the *x*-axis in Fig. 11. The *y*-axis of the intersection between the perpendicular line and the performance curve of the flooded-VRLA cell gives the hydrogen-evolution current. The value is 0.058 mA Ah^{-1}. Consequently, from Eq. (7), the oxygen-reduction current is found to be 0.572 mA Ah^{-1}. This gives an oxygen-recombination efficiency of 94.1% (i.e., the ratio of oxygen-reduction current to oxygen-evolution current).

From Eqs. (7) and (8), the hydrogen-evolution current at the negative plate is seen to be equal to the combined currents of grid corrosion at the positive plate and any evolved oxygen that is not subsequently reduced at the negative plate (uncombined-oxygen current), i.e.,

$$I_{H_2} = I_c + (I_{O_2} - I_{O_2\ reduction}) \quad (9)$$

Thus, the uncombined-oxygen current ($I_{O_2} - I_{O_2 reduction}$) is: 0.058–0.022 = 0.036 mA Ah^{-1}.

As mentioned in Section 3, the critical hydrogen-evolution current is determined at 100% oxygen-recombination efficiency. In other words, this current is calculated from the consumption of water due to grid corrosion, see Eq. (1). Since the oxygen-recombination efficiency of the VRLA cell examined here is 94.1%, the portion of the hydrogen-evolution current that is associated with grid corrosion is determined by subtracting the current due to uncombined-oxygen evolution from the total hydro-

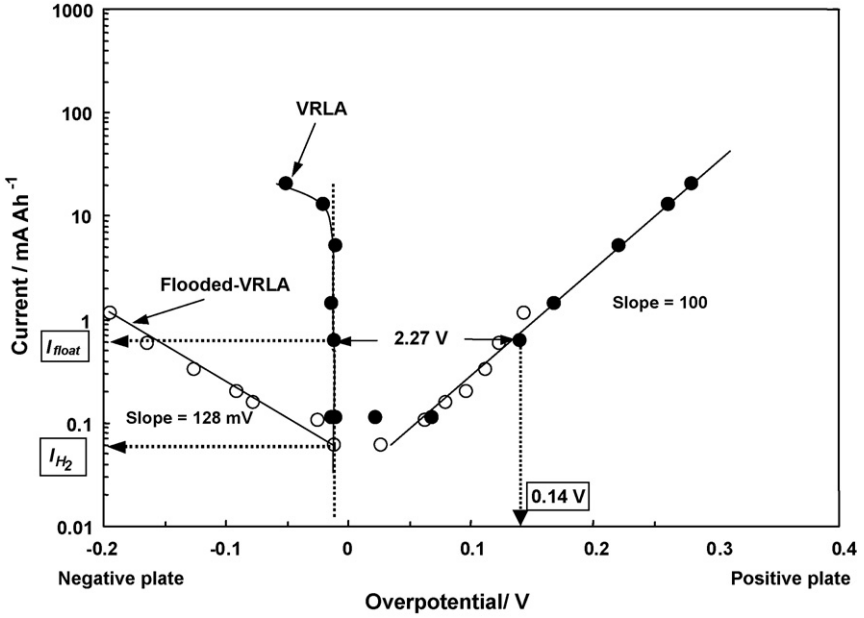

Fig. 11. Relationship between current and negative-plate/positive-plate overpotential in (○) flooded-VRLA and (●) VRLA cells at 21 °C.

Table 6
Comparison of critical values with measured values of float, hydrogen-evolution and oxygen-evolution currents.

Trial #	Measured value (mA Ah^{-1})			Δ(critical value – measured value) (mA Ah^{-1})		
	I_{float}	I_{H_2}	I_{O_2}	I_{float}	I_{H_2}	I_{O_2}
1	0.630	0.022	0.608	+0.370	+0.001	+0.369
2	1.346	0.028	1.318	−0.346	−0.005	−0.341
3[a]	0.722	0.024	0.698	+0.278	−0.001	+0.279
4	0.962	0.021	0.941	+0.038	+0.002	+0.036
5	1.019	0.041	0.978	−0.019	−0.018	−0.001
6	0.577	0.020	0.557	+0.423	+0.003	+0.420
7	0.659	0.010	0.649	+0.341	+0.013	+0.328
8	1.128	0.010	1.118	−0.128	+0.013	−0.141
9	0.612	0.011	0.601	+0.388	+0.012	+0.376
10	0.965	0.010	0.955	+0.035	+0.013	+0.022
11	0.635	0.022	0.613	+0.365	+0.001	+0.364
12	0.630	0.028	0.602	+0.370	−0.005	+0.375
13[b]	0.687	0.018	0.669	+0.313	+0.005	+0.308
14[c]	1.288	0.026	1.262	−0.288	−0.003	−0.285
15	1.125	0.020	1.110	−0.125	+0.003	−0.133
16	0.993	0.018	0.975	+0.007	+0.005	+0.002
17	1.299	0.021	1.278	−0.299	+0.002	−0.301
18	0.933	0.013	0.919	+0.067	+0.010	+0.058
19	0.687	0.020	0.667	+0.313	+0.003	+0.310
20	0.557	0.020	0.537	+0.443	+0.003	+0.440
21	0.862	0.027	0.835	+0.138	−0.004	+0.142
22	0.469	0.008	0.461	+0.531	+0.015	+0.516
23	1.130	0.028	1.102	−0.130	−0.005	−0.125
24	0.661	0.028	0.633	+0.339	−0.005	+0.344
25[b]	0.747	0.020	0.727	+0.253	+0.003	+0.250
26[c]	1.233	0.026	1.207	−0.233	−0.003	−0.230
27[d]	0.516	0.016	0.500	+0.484	+0.007	+0.477

[a] All elements at mid-levels.
[b] Repeat of trial #1.
[c] Repeat of trial #2.
[d] Repeat of trial #6.

gen current expressed by Eq. (9), i.e., 0.058–0.036 = 0.022 mA Ah^{-1}.

6.1.2. Float, hydrogen and oxygen currents of oxides doped with 16 elements

A similar procedure was used to determine the float current, the hydrogen-evolution current (associated with grid corrosion) and the oxygen-evolution current of cells using oxide doped with 16 residual elements at combined levels given by the 'first' Plackett–Burman design using the Upper Level (1) for each element (Table 2). The results (Table 6) show that all three currents are lower than their corresponding critical values in the undoped cell (trials #1, #13, #25) and the 12 doped cells (trials #4, #6, #7, #9 to #11, #16, #18 to #20, #22, #27). The remaining 12 doped cells give: (i) lower float and oxygen currents, but higher hydrogen (trials #3, #12, #21, #24); (ii) higher float and oxygen currents, but lower hydrogen current (trials #8, #15, #17); (iii) higher float and hydrogen currents, but lower oxygen current (trial #5); or (iv) higher float, oxygen and hydrogen currents (trials #2, #14, #23, #26). Although the doped cell in which all 16 elements are added at high levels (trial #2) delivers float, hydrogen and oxygen currents above the corresponding critical values, the differences are quite small. This indicates that Upper Level (1) for each element is reasonable.

6.1.3. Experimental reliability

In order to check the reliability of the data, a statistical analysis of the measured float, hydrogen and oxygen currents obtained for each set of repeated trials (see Table 6) was performed. Statistical theory shows that the distribution of a set of n measurements under identical experimental conditions can be assumed to follow a rule that is known as the 'normal law of error'. For each set, the individual measurements cluster more or less around the average value (Fig. 12), i.e., measurements that differ only a little from the average are more frequent than those that differ substantially from the average. The average value, m, is calculated by diving the sum of the individual values in a set by the number of measurements, i.e.,

$$m = \sum_{i=1}^{i=n} \frac{x_i}{n} \tag{10}$$

where x is the measured value and n is the number of measurements. The value of m will be the 'true average', μ, of the set if a very large number of measurements is conducted (i.e., if $n \to \infty$).

The relationship between the frequency of occurrence of a measurement and the amount by which it differs from the population average is shown in Fig. 12. The abscissa is expressed in units

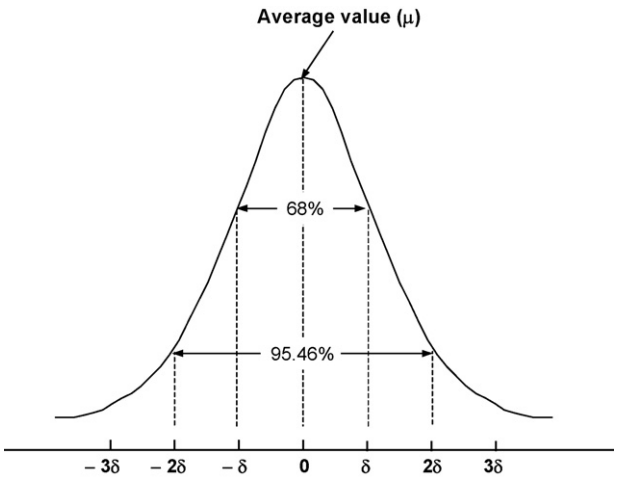

Fig. 12. Normal law of error.

Table 7
Statistical analysis of sets of repeated measurements.

Set #/Trial #	Measured value (mA Ah^{-1})		
	I_{float}	I_{H_2}	I_{O_2}
Set 1: repeats of control oxide			
1	0.630	0.022	0.608
13	0.687	0.018	0.669
25	0.747	0.020	0.727
28 (see Table 13)	0.778	0.020	0.758
Average, m	0.711	0.020	0.691
Variance	0.431×10^{-2}	2.700×10^{-6}	0.439×10^{-2}
Standard deviation, s	6.563×10^{-2}	1.630×10^{-3}	6.622×10^{-2}
Degrees of freedom	3	3	3
Set 2: repeats of oxide with all elements at high levels			
2	1.364	0.028	1.318
14	1.288	0.026	1.262
26	1.233	0.026	1.207
Average, m	1.289	0.027	1.262
Variance	0.319×10^{-2}	1.330×10^{-6}	5.550×10^{-2}
Standard deviation, s	5.651×10^{-2}	1.155×10^{-3}	3.960×10^{-2}
Degrees of Freedom	2	2	2
Set 3: repeats of trial #6			
6	0.577	0.020	0.557
27	0.516	0.016	0.500
Average, m	0.547	0.018	0.529
Variance	0.186×10^{-2}	8.000×10^{-6}	0.162×10^{-2}
Standard deviation, s	4.313×10^{-2}	2.828×10^{-3}	4.031×10^{-2}
Degrees of freedom	1	1	1
Pooled values			
Variance	0.353×10^{-2}	3.110×10^{-6}	0.349×10^{-2}
Standard deviation, s	5.940×10^{-2}	1.764×10^{-3}	5.908×10^{-2}
Uncertainty, ±	6.500×10^{-2}	1.930×10^{-3}	6.465×10^{-2}
Degrees of freedom	6	6	6

that represent the progressive deviation from the average value, namely, multiples of the standard deviation. The standard deviation at the peak of the graph is zero. The standard deviation, δ, is computed by using the following equation:

$$\delta = \left\{ \frac{(x_1 - m)^2 + (x_2 - m)^2 + (x_3 - m)^2 + \cdots + (x_n - m)^2}{n - 1} \right\}^{1/2} \quad (11)$$

where $(n–1)$ is the number of degrees of freedom in the set of measurements. The term $[(x_1 - m)^2 + (x_2 - m)^2 + (x_3 - m)^2 + \cdots + (x_n - m)^2]/(n - 1)$ is the variance. Thus, the standard deviation is the square root of the variance.

As mentioned above, 'true values' of the average and the standard deviation are obtained only from a very large set of measurements. In practice, however, this is not achievable because of time and cost restrictions. Accordingly, a small set of measurements is usually performed. The average value of a small set, m, will be spread around the true average, μ, of a very large set. (Note that, to avoid confusion, the symbols m and s are used to express the average value and the standard deviation of the small set of measurements, respectively.) Therefore, it is necessary to determine a procedure by which it is possible to make statements that will relate the average of a small set to the true average of the large set. This problem was solved in 1908 by W.S. Gosset, an English chemist, who introduced the factor, t. Multiplication of this factor by the ratio between the standard deviation and the square root of the number of measurements gives the uncertainty, U, of the average value m, as calculated by:

$$U = \frac{t \times s}{n^{1/2}} \quad (12)$$

The average, variance and standard deviation of three sets of repeated measurements are listed in Table 7. The first set is for trial #1 (control oxide) and its three repeats. The second set is for trial #2 (oxide doped with all 16 elements at high levels) and its two repeats. The third set is for trial #6 (oxide doped with 16 elements at various levels, see Table 3) and its one repeat. Since the number of degrees of freedom of each set is small, the uncertainties of the average values of individual sets will be large. Therefore, the pooled uncertainty of the three sets has been determined at the 95% confidence limit. At this limit, the uncertainties of the average values (based on six observations) of the float, hydrogen and oxygen currents are $\pm 6.500 \times 10^{-2}$, $\pm 1.930 \times 10^{-3}$ and $\pm 6.465 \times 10^{-2}$, respectively. These values will be used later to check the reliability of oxide containing 16 elements at their MALs, i.e., after determination of the MALs of the 16 elements, the float, hydrogen and oxygen currents of positive and negative plates prepared from the oxide with this new specification will be measured. The respective values of the three currents should be equal or less than 0.935 mA Ah^{-1} (i.e., critical value – uncertainty = 1.0000 – 0.06500), 0.021 mA Ah^{-1} (i.e., 0.023 – 0.00193) and 0.912 mA Ah^{-1} (i.e., 0.977 – 0.06465). If these conditions are met, it can be assured with 95% confidence that the oxide with advanced specification will deliver safe float, hydrogen and oxygen currents.

6.1.4. Determination of rates of change of individual elements

In order to obtain the concentration of each element at which the measured float, hydrogen and oxygen currents are equal to their corresponding critical values, it is necessary to determine the rate of change per unit concentration (ppm) of float, hydrogen and oxygen currents for each element. The trials (see Table 8) used to determine the rates of change in current caused by individual elements were those given in Table 6, except for trials #2 and #3 (16 elements at high- and mid-levels) and trials #13, #14, #25 to #27 (repeat trials). There are 10 trials for each element when its concentration is at a high level and 10 trials at a low level. For example, the concentration of copper at a high level (10 ppm) is defined by trials #4, #5, #7, #9, #16, #17, #19,

Table 8
Trials to determine the rate of change rate per unit concentration (ppm) of float, hydrogen and oxygen currents for individual elements.

Trial #	Ni	Sb	Co	Cr	Fe	Mn	Cu	Ag	Se	Te	As	Sn	Bi	Ge	Zn	Cd
1	0	0	0	0	0	0	0	0	0	0	0	0	0	0	0	0
4	10	10	0	0	10	3	10	20	0	0.3	0	10	0	0	0	0
5	10	0	0	5	10	3	10	0	1	0	10	0	0	0	0	500
6	0	0	10	5	10	3	0	20	0	0.3	0	0	0	0	500	500
7	0	10	10	5	10	0	10	0	1	0	0	0	0	500	500	0
8	10	10	10	5	0	3	0	20	0	0	0	0	500	500	0	500
9	10	10	10	0	10	0	10	0	0	0	0	10	500	0	500	500
10	10	10	0	5	0	3	0	0	0	0	10	10	0	500	500	0
11	10	0	10	0	10	0	0	0	0	0.3	10	0	500	500	0	0
12	0	10	0	5	0	0	0	0	1	0.3	0	10	500	0	0	500
15	10	0	10	0	0	0	0	20	1	0	10	10	0	0	500	500
16	0	10	0	0	0	0	10	20	0	0.3	10	0	0	500	500	500
17	10	0	0	0	0	3	10	0	1	0.3	0	0	500	500	500	500
18	0	0	0	0	10	3	0	20	1	0	0	10	500	500	500	0
19	0	0	0	5	10	0	10	20	0	0	10	10	500	500	0	500
20	0	0	10	5	0	3	10	0	0	0.3	10	10	500	0	500	0
21	0	10	10	0	10	3	0	0	1	0.3	10	10	0	500	0	500
22	10	10	0	5	10	0	0	20	1	0.3	10	0	500	0	500	0
23	10	0	10	5	0	0	10	20	1	0.3	0	10	0	500	0	0
24	0	10	10	0	0	3	10	20	1	0	10	0	500	0	0	0

#20, #23, #24, and at a low level (0 ppm) by trials #1, #6, #8, #10–#12, #15, #18, #21, #22. On averaging the trials for copper at a 10 ppm, the float (0.8579 mA Ah^{-1}), hydrogen (0.0218 mA Ah^{-1}) and oxygen currents (0.8361 mA Ah^{-1}) are obtained (Table 9); the remaining elements are at mid-levels. Similarly, on averaging the trials for copper at 0 ppm, the float (0.7954 mA Ah^{-1}), hydrogen (0.0180 mA Ah^{-1}) and oxygen (0.7778 mA Ah^{-1}) currents are obtained. When the copper concentration is raised from 0 to 10 ppm, the difference in float current is 0.0625 mA Ah^{-1}. Thus, the rate of change is 0.00625 mA Ah^{-1} per ppm if it is assumed that there is a linear relationship between float current and copper concentration. The corresponding rates of change in hydrogen and oxygen currents are 0.00038 and 0.00583 mA Ah^{-1} per ppm, respectively. Using a similar procedure, the rate of change in the float, hydrogen and oxygen currents for each of the remaining elements are calculated; the results are presented in Table 9.

With these rates, the levels at which the measured float, hydrogen and oxygen currents are equal to their corresponding critical values were calculated for each element. By way of example, the following analysis was conducted for copper.

The float, hydrogen and oxygen currents of copper, when its concentration is at high level (10 ppm), are 0.8579, 0.0218 and 0.8361 mA Ah^{-1}, respectively (Table 9). In order to increase these currents to the corresponding critical values, namely, 1.0000 (float), 0.0230 (hydrogen) and 0.9770 mA Ah^{-1} (oxygen) as given by Eqs. (2)–(4), the copper concentration should be increased from 10 ppm

Table 9
Rates of change of float, hydrogen and oxygen currents of 16 elements.

Elements	Level (ppm)	Average value (mA Ah^{-1})			Rate of change (mA Ah^{-1} per ppm)		
		I_{float}	$I_{hydrogen}$	I_{oxygen}	I_{float}	$I_{hydrogen}$	I_{oxygen}
Ni	10	0.9344	0.0192	0.9157	+0.02155	−0.00140	+0.02175
	0	0.7189	0.0206	0.6982			
Sb	10	0.7941	0.0171	0.7770	−0.00651	−0.00056	−0.00599
	0	0.8592	0.0227	0.8369			
Co	10	0.7946	0.0196	0.7755	−0.00641	−0.00006	−0.00629
	0	0.8587	0.0202	0.8384			
Cr	5	0.7821	0.0195	0.7626	−0.01782	−0.00016	−0.01774
	0	0.8712	0.0203	0.8513			
Fe	10	0.7415	0.0193	0.7221	−0.01958	−0.00014	−0.01951
	1.3	0.9118	0.0205	0.8918			
Mn	3	0.8963	0.0211	0.8751	+0.04643	+0.00080	+0.04543
	0	0.7570	0.0187	0.7388			
Cu	10	0.8579	0.0218	0.8361	+0.00625	+0.00038	+0.00583
	0	0.7954	0.0180	0.7778			
Ag	20	0.8665	0.0186	0.8483	+0.00498	−0.00016	+0.00517
	4	0.7868	0.0212	0.7656			
Se	1	0.8787	0.0224	0.8567	+0.10410	+0.00500	+0.09950
	0	0.7746	0.0174	0.7572			
Te	0.3	0.8114	0.0213	0.7901	−0.10167	+0.00933	−0.11233
	0	0.8419	0.0185	0.8238			
As	10	0.7973	0.0214	0.7764	−0.00587	+0.00030	−0.00611
	0	0.8560	0.0184	0.8375			
Sn	10	0.8463	0.0198	0.8269	+0.00393	−0.00002	+0.00399
	0	0.8070	0.0200	0.7870			
Bi	500	0.7611	0.0181	0.7429	−0.00026	−0.00001	−0.00026
	0	0.8922	0.0217	0.8710			
Ge	500	0.9291	0.0179	0.9111	+0.00041	−0.00001	+0.00042
	0	0.7242	0.0219	0.7028			
Zn	500	0.8189	0.0151	0.8042	−0.00003	−0.00002	−0.00001
	0	0.8344	0.0247	0.8097			
Cd	500	0.8932	0.0216	0.8721	+0.00027	+0.00001	+0.00026
	0	0.7601	0.0182	0.7418			

Table 10
Grouping of trials that deliver hydrogen current (mA Ah^{-1}) greater/lower than critical value.

Trial #	$I_{hydrogen}$	Ni	Sb	Co	Cr	Fe	Mn	Cu	Ag	Se	Te	As	Sn	Bi	Ge	Zn	Cd
5	0.041	H	L	L	H	H	H	H	L	H	L	H	L	L	L	L	H
23	0.028	H	L	H	H	L	L	H	H	H	H	L	H	L	H	L	L
24	0.028	L	H	H	L	L	H	H	H	H	L	H	L	H	L	L	L
12	0.028	L	H	L	H	L	L	L	L	H	H	L	H	H	L	L	H
21	0.027	L	H	H	L	H	H	L	L	H	H	H	H	L	H	L	H
Total trials		5	5	5	5	5	5	5	5	5	5	5	5	5	5	5	5
Frequency[a]		2	3	3	3	2	3	3	2	5	3	3	3	2	2	0	3
CV[b]	0.023																
11	0.022	H	L	H	L	H	L	L	L	L	H	H	L	H	H	L	L
17	0.021	H	L	L	L	L	H	H	L	H	H	L	L	H	H	H	H
4	0.021	H	H	L	L	H	H	H	H	L	H	L	H	L	L	L	L
15	0.020	H	L	H	L	L	L	L	H	H	L	H	H	L	L	H	H
19	0.020	L	L	L	H	H	L	H	H	L	L	H	H	H	H	L	H
6	0.020	L	L	H	H	H	H	L	H	L	H	L	L	L	L	H	H
20	0.020	L	L	H	H	L	H	H	L	L	H	H	H	H	L	H	L
16	0.018	L	H	L	L	L	L	H	H	L	H	H	L	L	H	H	H
18	0.013	L	L	L	L	H	H	L	H	H	L	L	H	H	H	H	L
9	0.011	H	H	H	L	H	L	H	L	L	L	L	H	H	L	H	H
8	0.010	H	H	H	H	L	H	L	H	L	L	L	L	H	H	L	H
10	0.010	H	H	L	H	L	H	L	L	L	L	H	H	L	H	H	L
7	0.010	L	H	H	H	H	L	H	L	H	L	L	L	L	H	H	L
22	0.008	H	H	L	H	H	L	L	H	H	H	H	L	H	L	H	L
Total trials		14	14	14	14	41	14	14	14	14	14	14	14	14	14	14	14
Frequency[a]		8	7	7	7	8	7	7	8	5	7	7	7	8	8	10	7

[a] Frequency of presence of a given element.
[b] Critical value.

to:

(i) float current
10 ppm + (1.0000 − 0.8579) mA Ah^{-1}/0.00625 mA Ah^{-1} ppm^{-1} = 32.736 ppm.
(ii) hydrogen current
10 ppm + (0.0230 − 0.0218) mA Ah^{-1}/0.00038 mA Ah^{-1} ppm^{-1} = 13.158 ppm.
(iii) oxygen current
10 ppm + (0.9770 − 0.8361) mA Ah^{-1}/0.00583 mA Ah^{-1} ppm^{-1} = 34.168 ppm.

Although there are three levels obtained for copper, the lowest level (i.e., ∼13 ppm) is taken as the MAL. This is because if either of the other two levels is chosen, the hydrogen current will be above its critical value.

From similar calculations, it was found that there are some elements (i.e., Ni, Sb, Co, Cr, Fe, Ag, As, Bi, Ge, Zn, see Table 9) for which the levels could not be determined because of the negative value of the rates of change, especially for hydrogen current. A negative rate of change of hydrogen current indicates that the hydrogen-evolution current decreases when the levels of these elements are increased. This is definitely not true for Ni, Sb and Co, however, as these elements are well known to promote hydrogen gassing. Furthermore, the above finding is contrary to observations made by ourselves [18] and by other authors [19–22] in previous studies when the three elements are added singularly, but not in combination with other elements as performed in the present work. This indicates that certain elements in the 16-member matrix have masked (or suppressed) the effects of Ni, Sb and Co on hydrogen gassing. Thus, it is important to identify the element, and/or group of elements, that can suppress the rates of hydrogen and oxygen evolution.

6.2. Determination of synergistic effects between elements

In order to determine the masking effects of elements, it is necessary to separate the experimental trials shown in Table 8 into two groups. One group delivers hydrogen currents that are greater than the critical value and the other group delivers currents that are lower than the critical value. The grouping of the experimental trials is presented in Table 10. In the absence of Zn (i.e., 0/5 frequency of presence), oxides containing Se (5/5), together with Ni, Ni and Co, or Sb and Co, always deliver hydrogen currents that are greater than the critical value (trials #5, #23, #24, #12, #21). This indicates that Zn has strong ability to suppress hydrogen gassing. Oxide containing Ni and Se gives the highest hydrogen current (i.e., 0.041 mA Ah^{-1}, trial #5), even when Cd is present at 500 ppm. This hydrogen current is much greater than the value given by oxide containing Se alone at a high level (0.0224 mA Ah^{-1}, Table 9) and also the value when the experiment is conducted with oxide containing Ni, Sb and Co all at 5 ppm (0.03 mA Ah^{-1}). This indicates that there is a detrimental synergy between nickel and selenium. Under these conditions, cadmium alone cannot suppress hydrogen gassing. The hydrogen current is, however, decreased from 0.041 to: (i) 0.028 mA Ah^{-1} (trial #23) in the presence of Ag and Ge; (ii) 0.021 mA Ah^{-1} (trial #17) in the presence of Bi, Ge, Zn and Cd; (iii) 0.020 mA Ah^{-1} (trial #15) in the presence of Ag, Zn and Cd; (iv) 0.008 mA Ah^{-1} (trial #22) in the presence of Ag, Bi and Zn. Furthermore, oxides containing Ni, Sb and Co also give low hydrogen currents only when Bi, Zn and Cd or Ag, Bi, Ge and Cd are present (trials #9 and #8). This suggests that Ag, Bi, Ge or Cd mask the hydrogen-gassing effects of Ni, Sb, Co and Se. The masking ability, however, becomes prominent when Ag, Bi, Ge and Cd are added collectively without/with Zn. The group of elements that provide the best masking effect is the combination of Ag, Bi and Zn.

It is well documented [18–22] that Ag, Ni, Co and Se promote oxygen gassing at positive plates. Therefore, it is also essential to examine any beneficial/detrimental synergistic effects between these 4 elements and any masking effects by the remaining 12 elements. Consequently, the above grouping process has also been performed for oxygen currents. The results are reported in Table 11. In the absence of Sb (i.e., 1/5 frequency of presence) and/or Fe (i.e., 1/5), oxides containing Ni (5/5), together with Se (4/5) and Cd or Co, Ag, Se and Cd always deliver oxygen currents above the critical value. For these elements, the oxide containing mainly Ni, Se and Cd gives the highest oxygen current (i.e., trial #17). The magnitude of the oxygen current decreases, however, below its critical value (0.977 mA Ah^{-1}) when either Sb or Fe, or both elements are present. In particular, the oxygen current decreases significantly

Table 11
Grouping of trials that deliver oxygen current (mA Ah^{-1}) greater or lower than critical value.

Trial #	I_{oxygen}	Ni	Sb	Co	Cr	Fe	Mn	Cu	Ag	Se	Te	As	Sn	Bi	Ge	Zn	Cd
17	1.278	H	L	L	L	L	H	H	L	H	H	L	L	H	H	H	H
8	1.118	H	H	H	H	L	H	L	H	L	L	L	L	H	H	L	H
15	1.110	H	L	H	L	L	L	L	H	H	L	H	H	L	L	H	H
23	1.102	H	L	H	H	L	L	H	H	H	H	L	H	L	H	L	L
5	0.978	H	L	L	H	H	H	H	L	H	L	H	L	L	L	L	H
Total trials		5	5	5	5	5	5	5	5	5	5	5	5	5	5	5	5
Frequency[a]		5	1	3	3	1	3	3	3	4	2	2	2	2	3	2	4
CV[b]	0.977																
16	0.975	L	H	L	L	L	L	H	H	L	H	H	L	L	H	H	H
10	0.955	H	H	L	H	L	H	L	L	L	L	H	H	L	H	H	L
4	0.941	H	H	L	L	H	H	H	H	L	H	L	H	L	L	L	L
18	0.919	L	L	L	L	H	H	L	H	H	L	L	H	H	H	H	L
21	0.835	L	H	H	L	H	H	L	L	H	H	H	H	L	H	L	H
19	0.667	L	L	L	H	H	L	H	H	L	L	H	H	H	H	L	H
7	0.649	L	H	H	H	H	L	H	L	H	L	L	L	L	H	H	L
24	0.633	L	H	H	L	L	H	H	H	H	L	H	L	H	L	L	L
11	0.613	H	L	H	L	H	L	L	L	L	H	H	L	H	H	L	L
12	0.602	L	H	L	H	L	L	L	L	H	H	L	H	H	L	L	H
9	0.601	H	H	H	L	H	L	H	L	L	L	L	H	H	L	H	H
6	0.557	L	L	H	H	H	H	L	H	L	H	L	L	L	L	H	H
20	0.537	L	L	H	H	L	H	H	L	L	H	H	H	H	L	H	L
22	0.461	H	H	L	H	H	L	L	H	H	H	H	L	H	L	H	L
Total trials		14	14	14	14	14	41	14	14	14	14	14	14	14	14	14	14
Frequency[a]		5	9	7	7	9	7	7	7	6	8	8	8	8	7	8	6

[a] Frequency of presence of a given element.
[b] Critical value.

to 0.461 mA Ah^{-1} (trial #22) even though the oxide contains elements, namely, Ni, Ag and Se, which are known to promote oxygen gassing. From these results, it can be concluded that Ni and Se also exert a detrimental synergistic effect on oxygen gassing. The effect is not, however, as strong as that for hydrogen evolution. Either Sb or Fe alone can mask the oxygen-gassing effects of Ni, Co, Ag and Se, but the strongest effect is found with a combination of these two elements.

A summary of the synergistic effects of the various residual elements in lead on hydrogen and oxygen evolution is presented in Fig. 13.

6.3. Second Plackett–Burman design

The above results show that most of the beneficial elements suppress the hydrogen-gassing effects of harmful elements such as Ni, Sb and Co. Thus, in order to determine the 'true' MALs of these elements, beneficial elements such as Bi, Zn and Cd should be removed in a second Plackett–Burman design (Table 12). Using the Upper Level (2) for each element (Table 12(a)), the complete Plackett–Burman design for seven elements at two concentrations is given in Table 12(b). The float, hydrogen and oxygen currents of the control oxide and oxides doped with seven elements were measured and the results are given in Table 13. Furthermore, since the MALs of As, Bi Cd, Fe, Sn, Tl and Zn still could not be obtained in combination (see Section 6.1.4), the individual MALs of these elements were determined singularly by adding each element alone to the control oxide. The results are summarised in Table 14. Using a procedure similar to that discussed in Section 6.1.4, the levels of seventeen elements at which the measured float, hydrogen and oxygen currents are equal to their corresponding critical values are calculated and the data are reported in Table 15. The individual MALs of these elements are determined according to the following considerations.

- For each element, there are three levels at which the measured float, hydrogen and oxygen currents are equal to the correspond-

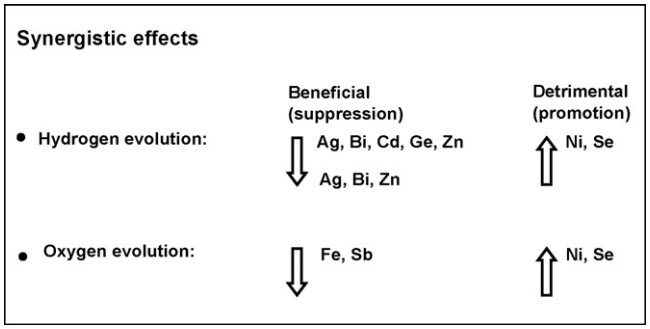

Fig. 13. Synergistic effects between elements.

Table 12
Second Plackett–Burman design: (a) Upper Level (2) for each element; (b) combination of seven elements in each trial.

Residual elements	Upper Level (2) (ppm)
(a)	
Ni	5
Sb	5
Co	5
Ag	80
As	15
Sn	80
Ge	500

Trial #	Ni	Sb	Co	Ag	As	Sn	Ge
(b)							
28[a]	0	0	0	0	0	0	0
29	5	5	5	80	15	80	500
30	2.5	2.5	2.5	40	7.5	40	250
31[b]	0	0	0	0	0	0	500
32	5	5	5	0	0	0	500
33	0	5	5	80	15	0	0
34	0	0	5	0	15	80	500
35	5	0	0	80	15	0	500
36	0	5	0	80	0	80	500
37	5	0	5	80	0	80	0
38	5	5	0	0	15	80	0

[a] Control oxide.
[b] Evaluating only the effect of germanium.

Table 13
Comparison of critical values with measured values of float, hydrogen and oxygen currents.

Trial #	Measured value (mA Ah^{-1})			Δ(critical value – measured value) (mA Ah^{-1})		
	I_{float}	$I_{hydrogen}$	I_{oxygen}	I_{float}	$I_{hydrogen}$	I_{oxygen}
28	0.778	0.020	0.758	+0.222	+0.003	+0.219
29	1.107	0.039	1.068	–0.107	–0.016	–0.091
30	0.804	0.011	0.793	+0.196	+0.012	+0.184
31	0.757	0.026	0.731	+0.243	–0.003	+0.246
32	1.141	0.013	1.128	–0.141	+0.010	–0.151
33	0.987	0.019	0.968	+0.023	+0.004	+0.009
34	0.991	0.011	0.979	+0.009	+0.012	–0.002
35	0.926	0.011	0.915	+0.074	+0.012	+0.062
36	0.676	0.012	0.664	+0.324	+0.011	+0.313
37	0.976	0.016	0.960	+0.024	+0.007	+0.017
38	0.982	0.010	0.972	+0.018	+0.013	+0.005

Table 14
Levels of elements at which measured float, hydrogen and oxygen currents are equal to their corresponding critical values.

Trial #	Elements	Upper Level (3) (ppm)	Measured value (mA Ah^{-1})			Level (ppm)		
			I_{float}	$I_{hydrogen}$	I_{oxygen}	I_{float}	$I_{hydrogen}$	I_{oxygen}
39	Tl	30	1.103	0.024	1.077	25	25	25
40	As	15	1.547	0.020	1.527	5	–	5
41	Bi	500	0.977	0.012	0.965	543	–	522
42	Cd	500	0.902	0.013	0.889	756	–	722
43	Fe	10	0.673	0.013	0.660	–	–	–
44	Sn	48	1.053	0.018	1.035	41	–	40
45	Zn	500	0.869	0.020	0.849	915	–	905

ing critical values. Nevertheless, the lowest level is taken as the MAL. For example, Ni has three levels, namely, 4 ppm for float current, 16 ppm for hydrogen current, and 4 ppm for oxygen current. Thus, the MAL of Ni is 4 ppm.

- Fe is chosen at 10 ppm even though this level is expected to be much lower than its 'true' MAL. This is because AGM separators are known to contain significant amounts of Fe. Thus, it is possible that the progressive leaching of this element from the separator during cycling could cause gassing problems if a high level is set for Fe in lead.
- The level of Ge is 10 ppm, even though its MAL is 250 ppm. This is because the hydrogen current for oxide doped with Ge at 500 ppm shows abnormal behaviour (Fig. 14). The hydrogen current is low initially, but increases sharply as the negative-plate overpotential shifts slightly to a more negative value. Consequently, Ge is not considered to be a beneficial element.
- The MALs of the beneficial elements Bi, Cd and Zn are estimated at 500 ppm, and that of Sn at 40 ppm. These decisions are due to the uncertainty of the level for each of these elements at which the measured hydrogen current reaches the critical value.

Table 15
Maximum acceptable levels (MALs) of residual elements.

Elements	Level (ppm)			MAL (ppm)
	I_{float}	$I_{hydrogen}$	I_{oxygen}	
Ni	4	16	4	4
Sb	6	5	6	5
Co	4	7	4	4
Cr	7	16	7	7
Fe	–	–	–	10
Mn	5	5	5	5
Cu	33	13	34	34
Ag	76	142	66	66
Se	2	1	2	1
Te	1.5	0.5	1.4	0.5
Tl	25	25	25	25
As	5	–	5	5
Sn	41	–	40	40
Bi	543	–	522	500
Ge	673	250	658	10
Zn	915	–	905	500
Cd	756	–	722	500

6.4. Proposed lead specifications for VRLA cells

From the MALs obtained for the individual seventeen elements, two specifications for lead are proposed, namely, specifications I and II (Fig. 15). The levels of the individual elements are based on the following considerations.

6.4.1. Specification I

- The levels of beneficial elements such as Bi, Cd and Zn are set at 500 ppm and that of Sn at 40 ppm.
- Most of detrimental elements are specified at the mid-levels, or slightly lower than the mid-levels of their corresponding MALs. This is because the oxide used to produce both the positive and negative plates is made from the same lead. Furthermore, there is a high risk of element migration between the two plate polarities during battery service. In the case of Co, for example, the MAL is 4 ppm and thus the specified level is 2 ppm. This is because, if the level was set at 4 ppm, the total level of Co at the negative

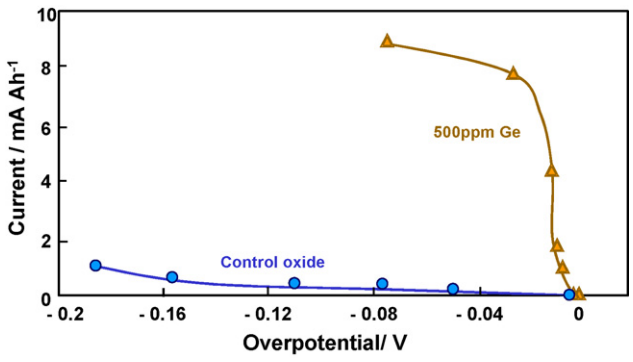

Fig. 14. Hydrogen-evolution currents of control oxide and oxide doped with germanium.

Proposed lead specifications

- With beneficial elements at high levels (Specification I)

	Ni	Sb	Co	Cr	Fe	Mn	Cu	Ag	Se	Te	As	Ge	Tl	Sn	Bi	Zn	Cd
	2	2	2	4	5	1.5	5	66	0.5	0.15	4	10	12	40	500	500	500
Standards:	2-10	5-20	ns	ns	10-30	ns	10-30	10-25	ns	ns	5-20	ns	ns				

- With beneficial elements at normal levels (Specification II)

Ni	Sb	Co	Cr	Fe	Mn	Cu	Ag	Se	Te	As	Ge	Tl	Sn	Bi	Zn	Cd
1	1	1	2	2.5	0.75	2.5	66	0.25	0.08	2	5	12	5 -10	5-25	10-20	5-10

Fig. 15. Proposal specifications for lead used to produce VRLA batteries.

plate could reach 8 ppm during service, due to migration from the positive plate, and this will exceed the MAL for the hydrogen current (i.e., 7 ppm). Under such a situation, the delivered hydrogen current would be greater than its critical value.
- Ag is set at its MAL (i.e., 66 ppm) because the total level of this element at the negative plate, even after complete migration, is still lower than the allowable level for the hydrogen current, viz., 142 ppm.

6.4.2. Specification II

- The levels of beneficial elements are reduced to the values normally found in refined lead, i.e., well below 500 ppm.
- Except for Ag, the levels of harmful elements in specification I are further decreased due to the negligible masking effects of the beneficial elements at their now reduced levels.
- Ag is still kept at 66 ppm. This is because, at this level, Ag does not affect oxygen and hydrogen gassing, even though the levels of the beneficial elements are reduced.

Two specifications for lead are proposed because some lead producers may not wish to add the beneficial elements at high levels. The next step is to examine the performance of positive and negative plates with active material produced from oxide using the proposed two specifications for lead.

6.5. Performance of negative and positive plates prepared from lead of specification I or II

6.5.1. Float, hydrogen and oxygen currents of oxides with proposed specifications

Several VRLA cells were constructed using control oxide and oxides doped with seventeen elements at the levels set in specifications I and II. The float, hydrogen and oxygen currents of these cells were determined at 21 and 45 °C, respectively. The charging capability of the negative and positive plates of the above cells during float service, particularly at elevated temperatures, was also evaluated

Current–voltage plots at 21 °C for flooded-VRLA and VRLA cells prepared from control oxide and oxides of either specification I or specification II are shown in Fig. 16. For the flooded-VRLA design, the cells using oxides of either specification I or II deliver higher current than that using control oxide. This is to be expected because the levels of residual elements in specifications I and II are set higher than those in the control oxide. There is little difference in the current response between cells that employ oxide of specification I and specification II, even though the levels of harmful elements in the former oxide are greater. The results demonstrate that the high levels of beneficial elements, i.e., Bi, Cd, Sn and Zn, have masked the adverse gassing effects of the harmful elements. For the VRLA design, there is no major difference in the current–voltage behaviour of all cells, irrespective of the degree of oxide purity examined in this study. In addition, there are no marked changes in current–voltage behaviour when cells are operated at a higher temperature of 45 °C, Fig. 17.

Using the data presented in Figs. 16 and 17, the float, hydrogen and oxygen currents were determined for the control oxide and oxides doped with 17 elements at the levels set in either specification I or II. The findings are reported in Table 16. At 21 °C, the cells prepared with doped oxides deliver higher float, hydrogen and oxygen currents than the cell using control oxide. Furthermore, the cell produced from oxide of specification I gives a similar hydrogen current, but higher float and oxygen currents, than the cell with oxide of specification II. The three currents for all cells are below their corresponding critical values. At 45 °C, the cell using oxide of spec-

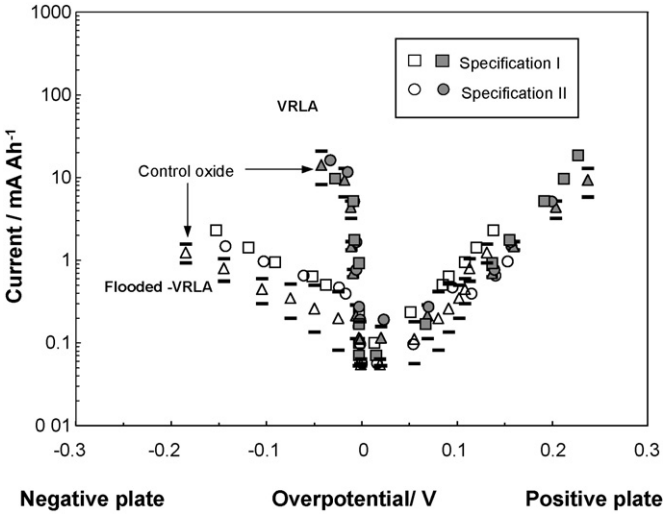

Fig. 16. Relationship between current and negative-plate/positive-plate overpotential at 21 °C for cells prepared from control oxide and from oxides of specification I or specification II.

Table 16
Measured values of float, hydrogen and oxygen currents of control oxide and oxides of specification I and II.

Oxide	Measured value (mA Ah^{-1})			Oxygen recomb. (%)	Δ(critical value – measured value) (mA Ah^{-1})		
	I_{float}	I_{H_2}	I_{O_2}		I_{float}	I_{H_2}	I_{O_2}
Under 21 °C							
Control	0.711	0.020	0.691	96	+0.289	+0.003	+0.286
Specification I	0.927	0.020	0.907	96	+0.073	+0.003	+0.070
Specification II	0.814	0.020	0.793	95	+0.186	+0.002	+0.184
Under 45 °C							
Control	7.512	0.150	7.362	95	–	–	–
Specification I	4.155	0.135	4.020	97	–	–	–
Specification II	8.946	0.145	8.701	95	–	–	–

ification I exhibits the lowest float, hydrogen and oxygen currents. On the other hand, the cell prepared with oxide of specification II shows an almost similar hydrogen current, but higher float and oxygen currents, than the control.

To date, the results show clearly that cells using oxides of either specifications I or II deliver satisfactory float, hydrogen and oxygen currents that are below their corresponding critical values. This is true even when the uncertainty of the experiment is taken into account, i.e., $\pm 6.500 \times 10^{-2}$, $\pm 1.930 \times 10^{-3}$, and $\pm 6.465 \times 10^{-2}$ for the corresponding float, hydrogen and oxygen currents, Table 7. The next step is to examine the charging capability of the above cells.

6.5.2. Conditions for selective discharge

During float service, lead-acid cells are maintained in a charged state for most of their operational time. In this condition, hydrogen evolution, oxygen evolution and grid corrosion occur in flooded-electrolyte cells, but are joined by oxygen reduction in VRLA counterparts. Although both designs operate differently, the requirements for float service are the same, namely, a low float current and minimal grid corrosion. These two criteria are imposed mainly to minimize water loss from the batteries. This is particularly important for VRLA cells which contain less acid than flooded-electrolyte counterparts. A further essential requirement, but often not realized, is that the negative and positive plates in lead-acid cells on float service should remain in a fully charged state; otherwise, the cells cannot provide full and stable capacity. In order to meet this prerequisite, the potential of the negative plate should be at more negative values during charging, and that of the positive plate at more positive values, than the corresponding equilibrium potentials ($E^{r}_{PbSO_4/Pb}$ and $E^{r}_{PbO_2/PbSO_4}$, respectively). In other words, the overpotential of the negative plate, $\eta_- = E^{i} - E^{r}_{PbSO_4/Pb}$, should be less than zero and that of the positive plate, $\eta_+ = E^{i} - E^{r}_{PbO_2/PbSO_4}$, should be greater than zero. It is known, however, that situations can arise whereby the overpotential of the negative plate becomes greater than zero so that the plate suffers 'selective discharge', or the overpotential of the positive plate becomes lower zero and thereby similarly undergoes 'selective discharge' [13]. It is therefore important to examine the changes in the overpotentials of negative and positive plates during overcharge in cells using control oxide and oxides of specifications I or II.

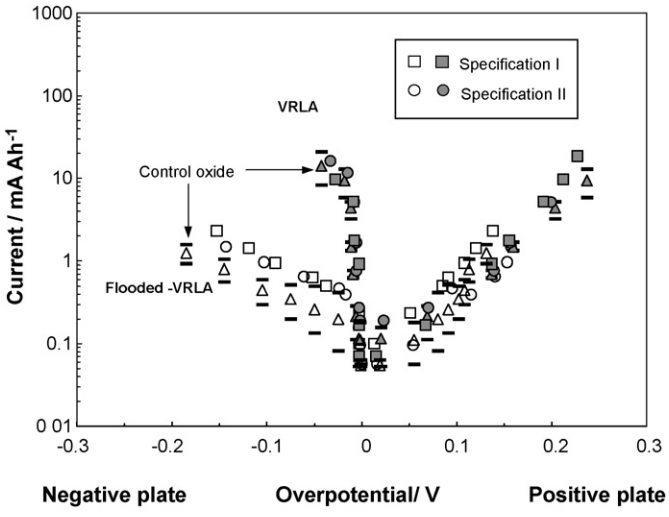

Fig. 17. Relationship between current and negative-plate/positive-plate overpotential at 45 °C for cells prepared from control oxide and from oxides of specification I or specification II.

6.5.2.1. Selective discharge of negative plate. During overcharging, the potentials of the positive and negative plates shift so that the same amount of current flows through both polarities. In a practical VRLA cell (i.e., low hydrogen-evolution rate), the current consumed by hydrogen evolution at the negative plate equals the sum of that consumed by grid corrosion and any uncombined oxygen at the positive plate. Furthermore, this condition is achieved at a negative-plate potential that is at more negative values than its equilibrium value. An unbalanced VRLA cell can result from excessive evolution of hydrogen through contamination of the negative material with impurities. This is shown schematically in Fig. 18; to assist the explanation, current–potential curves for the discharge and the charge reactions of the negative plate are also included. The contamination may originate from the starting leady oxide and/or from the electrolyte. On subjecting the cell to constant-voltage charging, the potential of the negative plate will shift towards more positive values in order to balance the current flow through both polarities. If the current consumed by hydrogen evolution at the negative plate is still greater than that consumed by grid corrosion and any uncombined oxygen at the positive plate, the negative-

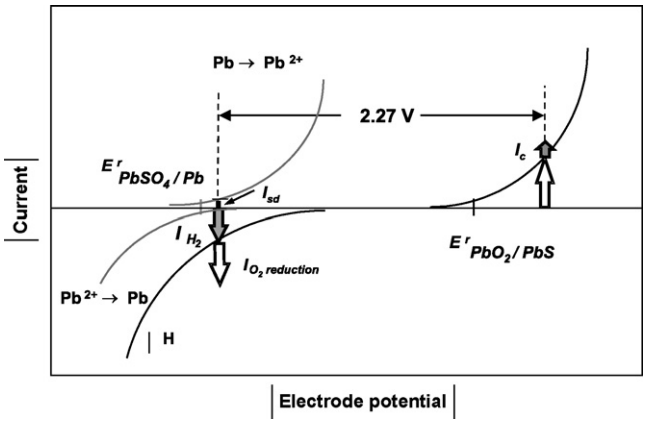

Fig. 18. Selective discharge of negative plate in VRLA cell during constant-voltage charging.

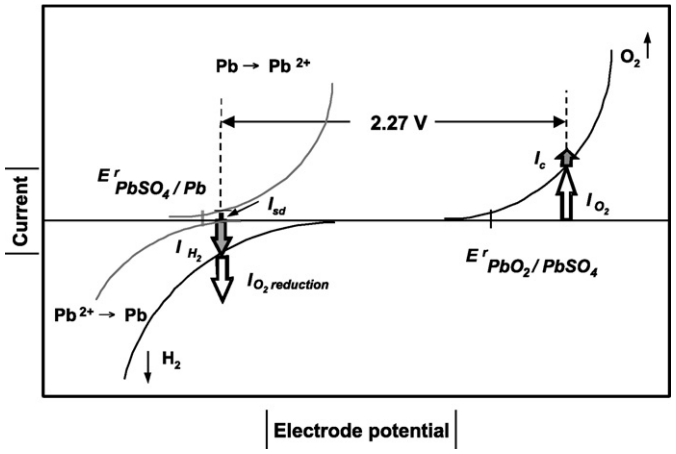

Fig. 19. Selective discharge of positive plate in VRLA cell during constant-voltage charging.

plate potential will be driven to a value that is more positive than the equilibrium potential. In such a situation, the current will be balanced by selective discharge (I_{sd}, Fig. 18) of the negative plate via the following reaction couple:

$$2H^+ + 2e^- \rightarrow H_2 \quad (13)$$

$$Pb + H_2SO_4 \rightarrow PbSO_4 + 2H^+ + 2e^- \quad (14)$$

Obviously, the rate of hydrogen evolution in a VRLA cell exerts a strong influence on the selective discharge of the negative plate. The discharge is intensified if the battery uses a highly corrosion-resistant grid alloy, and/or has a very high oxygen-recombination efficiency (e.g., as a result water loss during prolonged operation).

6.5.2.2. Selective discharge of positive plate. When the rate of oxygen evolution at the positive plate is enhanced (e.g., through the influence of impurities) and the efficiency of oxygen reduction at the negative is low, i.e., <80%, the positive-plate potential will decrease towards the equilibrium value in order to provide the same flow of current through each plate polarity (Fig. 19). If the potential of the positive plate moves to a value more negative than the equilibrium potential and the combined current due to the oxygen evolution and grid corrosion is still higher than that consumed by oxygen reduction and hydrogen evolution at the negative plate, then the difference will be taken up by selective discharge of the positive plate via the following reaction couple:

$$2H_2O \rightarrow O_2 + 4H^+ + 2e^- \quad (15)$$

$$PbO_2 + 2H^+ + H_2SO_4 + 2e^- \rightarrow PbSO_4 + 2H_2O \quad (16)$$

The rate of selective discharge will be increased further if the positive plate uses a grid alloy that is more susceptible to corrosion.

Clearly, the negative plate or the positive plate in a VRLA cell can only become selectively discharged when the overpotential is equal/greater than zero or equal/less than zero, respectively, i.e., $\eta_- \geq 0$, $\eta_+ \leq 0$. Thus, the possibility of selective discharge can be confirmed by measurement of the plate overpotentials during overcharging at various constant voltages.

6.5.3. Charging capability of VRLA cells produced from control oxide and oxides with proposed specifications

6.5.3.1. Change in overpotential of negative and positive plates during overcharge. When charging VRLA cells at 21 °C with voltages up to 2.30 V, the potential of negative plate remains close to its equilibrium value, i.e., −0.003 to −0.020 V (Fig. 20). Obviously, there is a corresponding marked increase in the overpotential of the positive plate. With further increase in the charging voltage (i.e., >2.30 V),

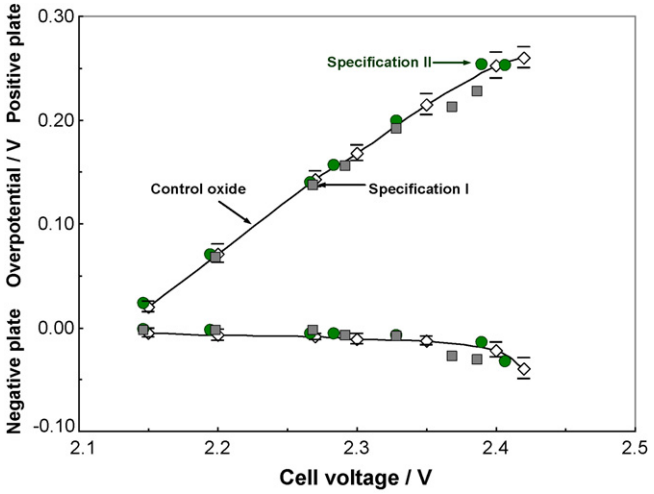

Fig. 20. Change in negative-plate and positive-plate overpotentials during overcharge at 21 °C.

the absolute values of the overpotential of both plate polarities increase, but that of the positive plate starts to level off at a voltage greater than 2.4 V. The change in plate overpotentials is similar in all cells, irrespective of the oxide used, i.e., control oxide, oxide of specification I, or oxide of specification II.

The change in overpotentials of negative and positive plates in VRLA cells at 45 °C is presented in Fig. 21. For each cell, the negative-plate overpotential decreases slightly when the voltage is increased up to 2.25 V; there is a corresponding marked increase in the overpotential of the positive plate. With further increase in charging voltage, however, the overpotential of the negative plate decreases at a greater rate than that of the positive plate. In addition, the overpotential of the positive plate starts to level off at cell voltage greater than 2.35 V. As observed at 21 °C, all cells display similar overpotential behaviour. Nevertheless, the difference in the absolute value of the overpotentials at the negative plate is greater, and that at the positive plate is smaller, in cells operated at 45 °C. Since the absolute value of the overpotential at the negative plate increases with increase in temperature, the negative plate will accept charge more effectively at elevated temperature. By contrast, the positive plate will receive charge less efficiently at elevated temperature because of the decrease in overpotential. This

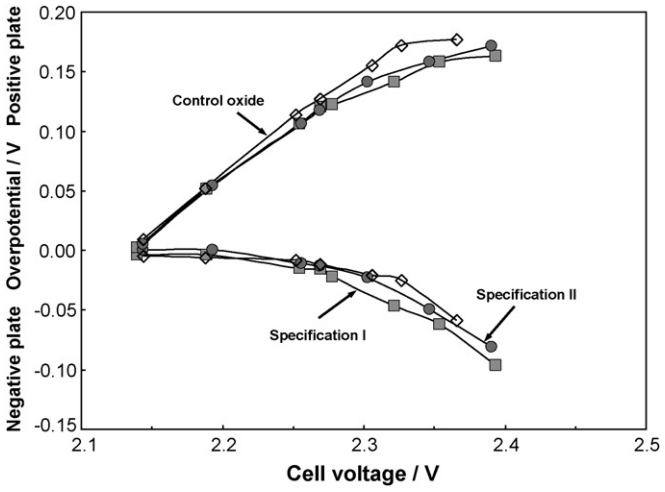

Fig. 21. Change in negative-plate and positive-plate overpotentials during overcharge at 45 °C.

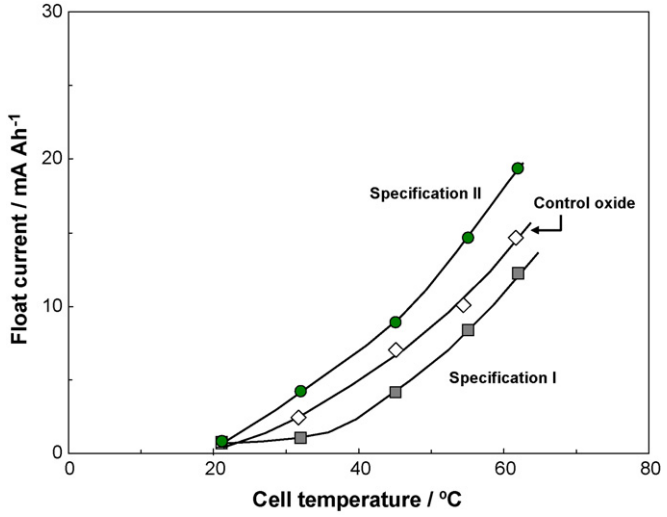

Fig. 22. Effect of temperature on float current of VRLA cells made from different oxides.

observation is in good agreement with the general acceptance that charging efficiency is better for negative plates than for positive plates at high temperature.

In practice, VRLA cells are usually charged at a voltage limit between 2.20 and 2.45 V. In this voltage range, the negative-plate overpotentials of cells using control oxide and oxides of specification I or specification II are between −0.01 and −0.05 V at 21 °C (Fig. 20) and −0.01 and −0.1 V at 45 °C (Fig. 21). Furthermore, the oxygen-recombination efficiencies of the cells are very high (i.e., 95–97%). Thus, it can be concluded that under prolonged float or normal charging conditions, these VRLA cells do not succumb to selective discharge of either the negative or the positive plates.

6.5.3.2. Float current. The change in float current with temperature of VRLA cells using control oxide and oxides of either specification I or specification II is shown in Fig. 22. For all cells, i.e., irrespective of the type of oxide employed, the float current is found to increase with cell temperature. The cell using oxide of specification I gives the lowest current and that using oxide of specification II the highest currents with increase in temperature.

7. Key outcomes

This study has identified the 'safe' levels for the residual elements in lead used to produce oxide for VRLA batteries that operate in standby applications such as telecommunications and uninterruptible power-supply systems.

- Seventeen elements have been examined, namely: antimony, arsenic, bismuth, cadmium, chromium, cobalt, copper, germanium, iron, manganese, nickel, selenium, silver, tellurium, thallium, tin, and zinc. Bismuth, cadmium, tin and zinc are considered 'beneficial elements' for VRLA batteries as these elements have little effect on gassing. The remaining elements are 'harmful elements' because they promote hydrogen- and/or oxygen-gassing rates.
- Critical values for the float, hydrogen and oxygen currents have been calculated from a field survey of battery failure data. These values serve as a base-line for comparison with the corresponding measured currents from cells using positive and negative plates produced either from the control oxide or from oxide doped with different levels of the 17 elements in combination.
- The Plackett–Burman experimental design has been adopted to obtain efficient screening of the seventeen elements in combination.
- The levels at which the measured float, hydrogen and oxygen currents are equal to their corresponding critical values have been determined for each residual element. The lowest value is taken as the maximum acceptable level (MAL) of that element.
- Synergistic effects have been found during the determination of the MALs of individual elements. For hydrogen gassing, masking effects ('beneficial synergistic effects') arise mainly from the combined action of bismuth, cadmium, germanium, silver, and zinc. A combination of bismuth, silver and zinc gives the greatest suppression of gassing, whereas nickel and selenium accelerate the gassing rate markedly. This indicates that nickel and selenium exert a 'detrimental synergistic effect' on hydrogen evolution. For oxygen gassing, masking effects come from the combined action of antimony and iron. Again, nickel and selenium are found to enhance the gassing rate, but the effect is not as strong as that observed for hydrogen evolution.
- Two specifications – specification I and specification II – for the 17 elements in lead have been developed through this systematic and thorough exercise. The beneficial elements are set at high levels in specification I, and at normal levels in specification II. Furthermore, the levels of most of the harmful elements in specification I are twice as high as those in specification II.
- VRLA cells using positive and negative plates produced from oxide of either specification I or II deliver satisfactory float, hydrogen and oxygen currents, i.e., below the corresponding critical values. Furthermore, these cells do not suffer from selective discharge of the negative or positive plates during float charging at constant voltage. The set voltage can be as low as 2.20 V, even when oxygen recombination has become very efficient.
- The float current of VRLA cells increases with increase in temperature, irrespective of the type of oxide. Nevertheless, the degree of increase in float current is greater when using oxide of specification II. This demonstrates that by keeping the beneficial elements at high levels, greater concentrations of harmful elements can be tolerated. Moreover, the effect of temperature on the float current delivered by oxide of specification I is even smaller than that observed for the control oxide.

Acknowledgements

The authors are grateful to the Advanced Lead-Acid Battery Consortium, Durham, NC, USA for supporting this work and for permission to publish the results.

References

[1] D. Berndt, W.E.M. Jones, Proceedings INTELEC'98, San Fransico, USA, 1998, pp. 443–451.
[2] W.E.M. Jones, D.O. Feder, Proceedings TELESCON'97, Budapest, Hungary, 1997, pp. 295–303.
[3] W. Brecht, Batteries Int. 30 (1997), 62, 63, 66.
[4] W.E.M. Jones, D.O. Feder, Batteries Int. 33 (1997), 80, 77, 79, 83.
[5] M.W. Stevenson, J.E. Manders, S. Eckfeld, R.D. Prengaman, J. Power Sources 107 (2002) 146–154.
[6] W.B. Brecht, Batteries Int. 20 (1994) 40–43.
[7] J.S. Symanski, B.K. Mahato, K.R. Bullock, J. Electrochem. Soc. 135 (1988) 548–551.
[8] A.I. Harrison, Proceedings INTELEC'97, Melbourne, Australia, 1997, pp. 238–243.
[9] W.E.M. Jones, H.A. Vanasse, C.E. Sabotta, J.E. Clapper, E.F. Price, Proceedings INTELEC'98, San Fransico, USA, 1998, pp. 461–469.
[10] F. Vaccaro, J. McAndrews, Proceedings INTELEC'97, Melbourne, Australia, 1997, pp. 403–406.
[11] R.D. Prengaman, J. Power Sources 42 (1993) 25–33.
[12] R.L. Plackett, J.P. Burman, Biometrika 33 (1946) 305–325.
[13] L.T. Lam, N.P. Haigh, C.G. Phyland, N.C. Wilson, D.G. Vella, L.H. Vu, D.A.J. Rand, J.E. Manders, C.S. Lakshmi, Proceedings INTELEC'98, San Fransico, USA, 1998, pp. 452–460.

[14] P. Ruetschi, R.T. Angstadt, B.D. Cahan, J. Electrochem. Soc. 106 (1959) 547–551.
[15] S. Fletcher, D.B. Matthews, J. Appl. Electrochem. 11 (1981) 23–32.
[16] J.A. Magyar, M.A. Kepros, R.F. Nelson, J. Power Sources 31 (1990) 93–106.
[17] P.K. Ng, Proceedings INTELEC'97, Melbourne, Australia, 1997, pp. 529–532.
[18] L.T. Lam, J.D. Douglas, R. Pillig, D.A.J. Rand, J. Power Sources 48 (1994) 219–232.
[19] B.K. Mahato, W.H. Tiedemann, J. Electrochem. Soc. 130 (1983) 2139.
[20] H. Sanchez, Y. Meas, I. Gonzales, M.S. Quiroz, J. Power Sources 32 (1993) 43–53.
[21] M. Maja, N. Penzzi, J. Power Sources 22 (1988) 1–9.
[22] J.R. Pierson, C.E. Weinlein, C.E. Wright, in: D.H. Collins (Ed.), Power Sources 5. Research and Development in Non-Mechanical Electrical Power Sources, Academic Press, New York, 1975, p. 97.